

# Pterosaurs from the Late Cretaceous of Angola

Alexandra E. Fernandes <sup>1,2,3,\*</sup> , Octávio Mateus <sup>1,2</sup> , Brian Andres <sup>4</sup> , Michael J. Polcyn <sup>5</sup>, Anne S. Schulp <sup>6,7</sup> , António Olímpio Gonçalves <sup>8</sup> and Louis L. Jacobs <sup>5</sup>

<sup>1</sup> Museu da Lourinhã, 2530-158 Lourinhã, Portugal

<sup>2</sup> GEOBIOTEC, Department of Earth Sciences, NOVA School of Science and Technology, Universidade NOVA de Lisboa, Campus de Caparica, 2825-149 Caparica, Portugal

<sup>3</sup> SNSB, Bayerische Staatssammlung für Paläontologie und Geologie, 80333 Munich, Germany

<sup>4</sup> Department of Animal & Plant Sciences, University of Sheffield, Sheffield S10 2TN, UK

<sup>5</sup> Roy M. Huffington Department of Earth Sciences, Southern Methodist University, Dallas, TX 75205, USA

<sup>6</sup> Naturalis Biodiversity Center, 2333 CR Leiden, The Netherlands

<sup>7</sup> Faculty of Geosciences, Utrecht University, 3584 CB Utrecht, The Netherlands

<sup>8</sup> Departamento de Geologia, Faculdade de Ciências, Universidade Agostinho Neto, 374J+R8F, Luanda, Angola

\* Correspondence: ae.fernandes@campus.fct.unl.pt

**Abstract:** Here, we describe the first pterosaur remains from Angola, an assemblage of fourteen bones from the Lower Maastrichtian marine deposits of Bentiaba, Namibe Province. One new species is introduced, *Epapatelo otyikokolo*, gen. et sp. nov., which comprises an articulated partial left humerus and ulna as well as an articulated left ulna and radius (from a second individual). Phylogenetic analysis confirms a non-nyctosaurid pteranodontian attribution for this new taxon and supports a new apomorphy-based clade, Aponyctosauria, which is here defined. Late Cretaceous pteranodontians are rare in Sub-Saharan Africa and throughout the Southern Hemisphere. Preliminary histological analysis also reveals a likely sub-adult age for one of the specimens. This fossil assemblage provides a first glimpse of Angolan pterosaur paleobiodiversity providing further insight into the Gondwanan ecosystems of the Upper Cretaceous.



**Citation:** Fernandes, A.E.; Mateus, O.; Andres, B.; Polcyn, M.J.; Schulp, A.S.; Gonçalves, A.O.; Jacobs, L.L. Pterosaurs from the Late Cretaceous of Angola. *Diversity* **2022**, *14*, 741. <https://doi.org/10.3390/d14090741>

Academic Editor: Eric Buffetaut

Received: 24 July 2022

Accepted: 5 September 2022

Published: 9 September 2022

**Publisher's Note:** MDPI stays neutral with regard to jurisdictional claims in published maps and institutional affiliations.



**Copyright:** © 2022 by the authors. Licensee MDPI, Basel, Switzerland. This article is an open access article distributed under the terms and conditions of the Creative Commons Attribution (CC BY) license (<https://creativecommons.org/licenses/by/4.0/>).

**Keywords:** pterosauria; pteranodontia; *Epapatelo otyikokolo*; Cretaceous; Maastrichtian; Gondwana; Angola; Namibe Basin

## 1. Introduction

Pterosaurs were the first vertebrates to have evolved powered flight. They were a highly successful and diverse group, with a global distribution throughout nearly their entire temporal range, from the Late Triassic through the Cretaceous [1]. Here, we present a morphological description and classification for fossil pterosaur material collected in the present-day African country of Angola, increasing the recognized diversity of Late Cretaceous Gondwanan communities.

Pterosaur discoveries in Africa have been relatively sparse, with main fossil concentrations on the continent occurring in northern countries, and disparate occurrences occurring further south. This distribution is likely due to sparse field sampling and the potential unavailability of Mesozoic exposures throughout sub-Saharan Africa. In addition, the majority of what has been unearthed across Africa thus far are found as isolated bones [2]. Most localities are Cretaceous in age, with some Jurassic sites as well (Table S1). The specimens described here were collected during several expeditions carried out by Projecto PaleoAngola members, who collected fossils throughout multiple field seasons in various localities, beginning in 2005 and continuing up until the present day [3]. These efforts have been greatly successful in increasing known Late Cretaceous taxonomic diversity (including new species) of dinosaurs, marine reptiles, turtles, fish, [3–13], and now here in greater detail, pterosaurs.

## 2. Materials and Methods

All pterosaur mechanical specimen preparation was completed at the laboratory of the Museu da Lourinhã in Lourinhã, Portugal and at the Universidade Nova de Lisboa in Lisbon, Portugal, using a PaleoTools ME-9100 for the bulk removal of the surrounding matrix, a PaleoTools Micro Jack 6 for more precise matrix removal, and a variety of metal manual tools and wooden dowels for precision work. Throughout this process, all bone surfaces were consolidated with 5% Paraloid B-72 diluted in acetone, and any breaks or deep fissures were glued and reinforced with 20% or 50% Paraloid B-72 as required. Bones were then compound blue light scanned using an Artec Space Spider, and all scans were processed using Artec Studio 14. All digital material is available in Morphobank Project 3966 [14].

Phylogenetic analysis was conducted using TNT version 1.5 [15,16] using the matrix by Longrich et al. 2018 [17], which added new characters to the Andres et al. 2014 [18] matrix and also includes additional taxa from the Late Cretaceous. The matrix contains continuous and discrete partitions. Four outgroups were used with *Euparkeria capensis* Broom 1913 [19] as the primary outgroup. The matrix incorporates ordered and unordered characters. It should be noted that TNT begins numbering characters and taxa from 0. All characters were equally weighted, although the continuous characters were rescaled from a minimum of 0.000 to a maximum of 1.000 so that their maximum change would equal the maximum change along a branch of a binary character (i.e., one step). Ambiguous branch support was not used, zero-length branches were automatically collapsed, and the resultant trees were filtered for the best score. A basic traditional tree-search analysis was conducted with 1000 random addition sequence replicates (an alternate analysis was run with the ratchet, yielding identical results and so found to be unnecessary). Analytical protocols are expanded upon in the supplementary material of Andres et al. 2014 [18]. No new characters were added to the matrix here, although character 236 for *Cretornis hlavaci* Frič, 1881 [20] was recoded to address the misidentification of the distal tuberculum by Averianov and Ekrt [21]. *Piksi barbarulna* Varricchio 2002 [22] is not considered a pterosaur here and so was omitted from the analysis. One new taxon was added and analyzed, represented by combining characters from the holotype-articulated MGUAN-PA650 humerus and MGUAN-PA650 ulna (material from the most complete individual and exhibiting the most characters) and the paratype-articulated MGUAN-PA661 ulna and radius and was named “Epatatelo\_otyikokolo” (MGUAN-PA: Museu Geológico Universidade Agostinho Neto—Projecto PaleoAngola).

Paleohistological sample preparation was conducted in the laboratory of the Rheinische Friedrich-Wilhelms-Universität Bonn in Bonn, Germany, to create thin sections by slicing bone and embedding the sample in Araldite 2020/A clear adhesive epoxy catalyzed with Araldite 2020/B epoxy resin to facilitate handling. A circular rotating diamond-tipped disc saw blade on a Buehler Isomet precision sectioning saw was used to cut and section the block and sample. The samples were wet-ground using a Jean Wirtz TF 250 metallographic polishing machine fitted with abrasive paper. Using the method described by Lamm [23], they were further wet-ground with silicon carbide grinding powder and water on glass plates of decreasing coarseness levels, beginning with F220 grit and then stepping to F400 and F600 grit, prior to covering with a slide cover. For histological analysis, the thin sections were analyzed with a Nikon Eclipse E400 POL petrographic microscope under normal light, under crossed plane polarized light, and through a lambda filter at the Universidade Nova de Lisboa.

The material described here is on temporary loan from the Geological Museum of Universidade Agostinho Neto, Luanda, Angola, to the Museu da Lourinhã, Lourinhã, Portugal. All necessary permits were obtained for the described study, which complied with all relevant regulations.

### 3. Nomenclatural Acts

The electronic edition of this article conforms to the requirements of the amended International Code of Zoological Nomenclature, and hence, the new names contained herein are available under that code from the electronic edition of this article. This published work and the nomenclatural acts it contains have been registered in ZooBank, the online registration system for the ICZN. The ZooBank LSIDs (Life Science Identifiers) can be resolved, and the associated information can be viewed through any standard web browser by appending the LSID to the prefix "<http://zoobank.org/>". The LSID for this publication is: urn:lsid:zoobank.org:pub:1ca78d69-eb55-4ad7-9fd1-e03058127604. The electronic edition of this work was published in a journal with an ISSN and has been archived and is available from the following digital repositories: PubMed Central and LOCKSS.

### 4. Geographical and Geological Setting

The Republic of Angola, on the west coast of southern Africa (Figure 1), is home to the arid Namibe desert region and has abundant fossiliferous outcrops. By the late Maastrichtian, Angola's present-day coastline had already formed, and Africa had essentially become isolated from other continental landmasses, meaning that inhabitant species were able to be further endemically specialized into their own unique paleobiology [24,25].

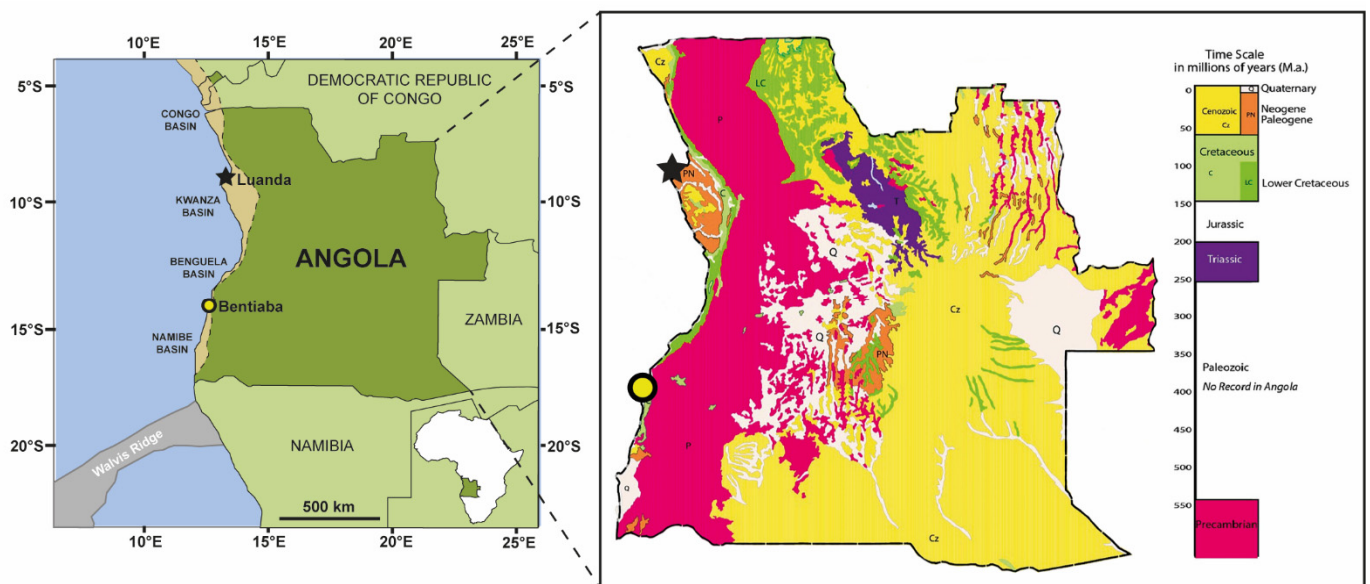


**Figure 1.** Location of the commune of Bentiaba with a geological map of Angola. Adapted from Strganac et al. 2014 [26] and Mateus et al. 2019 [3], according to the U. S. Geological Survey 2002 (scale: 1:30,000,000) [27].

The fossiliferous Cretaceous coastline outcrops of the Namibe desert region are mainly composed of marine clastics. Marine reptile-bearing sandstones sit atop a basalt complex, the Ombe Volcanic Formation, dated at 84.6 Ma [28] (Figure 2). Above the Ombe Formation are the Baba Formation followed by the Mocuio Formation, which encompass the Bentiaba locality (Figure 1). Based on vertebrate and invertebrate faunas [12] as well as on carbon and oxygen isotope analyses, magnetostratigraphy, and  $^{40}\text{Ar}/^{39}\text{Ar}$  dates for the section at Bentiaba [28], the age of this locality is dated to the early Maastrichtian, binned within the 71.64–71.40 Ma interval [28].

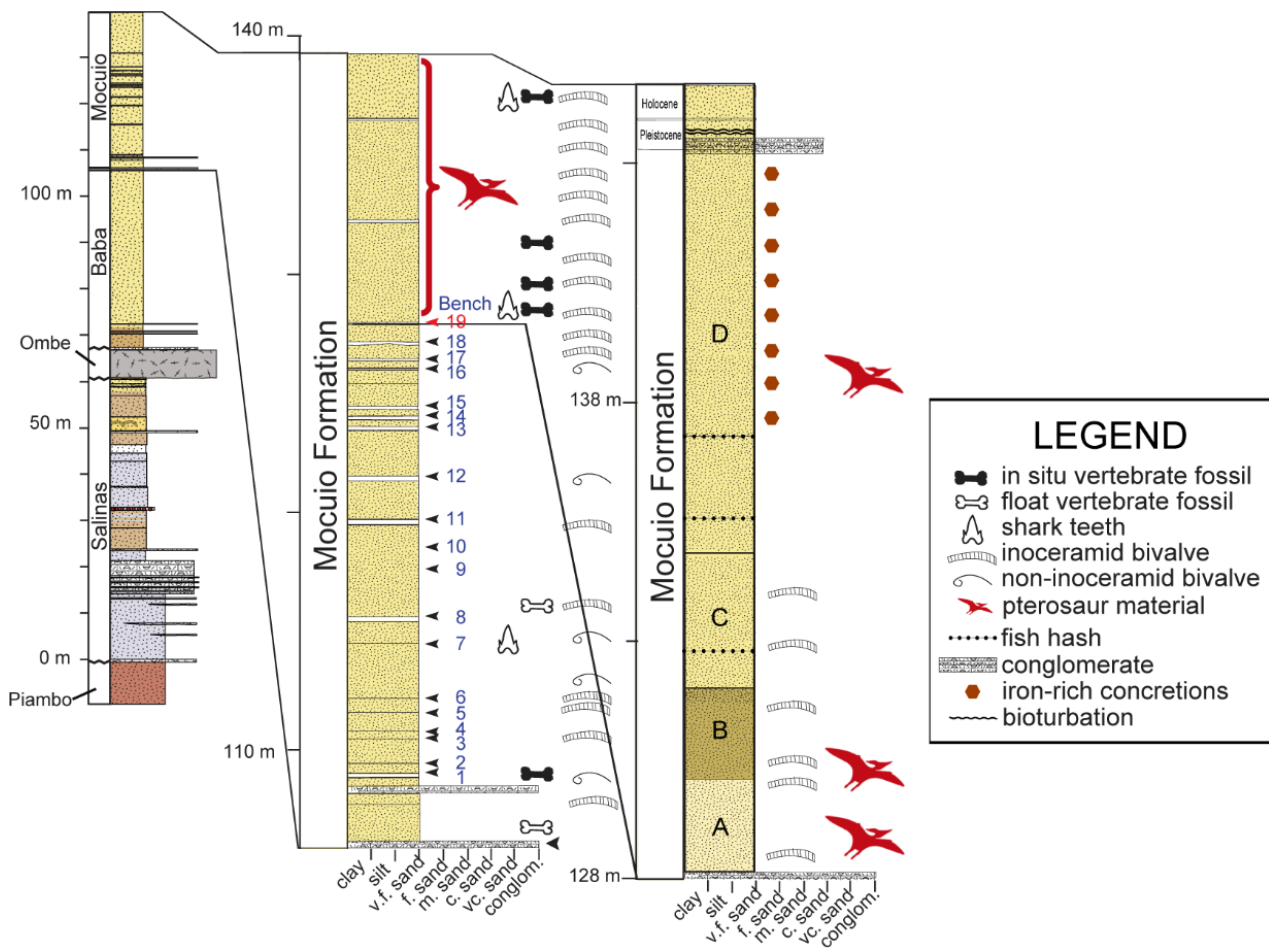


**Figure 2. Stratigraphic section of the Bentiaba locality.** Strata yielding pterosaur fossils are demarcated (modified from Strganac et al. 2014 [26]).

Within Angola, pterosaur material has so far only been collected from the site of Bentiaba. The eleven(?) pterosaur individuals discussed herein were collected from a 0.15 km<sup>2</sup> area within the same stratigraphic level, although they were not found in association. Three articulated sets of pterosaur remains were discovered: MGUAN-PA650 comprises a left humerus distal fragment articulated with a complete ulna, MGUAN-PA654 comprises a right metacarpal IV distal fragment articulated with a digit IV first phalanx proximal fragment, and MGUAN-PA661 comprises a left ulna articulated with a radius. Eight other elements were found in isolation.

The lithology of Bentiaba is characterized by fine-grained pinkish-white to reddish-yellow sandstone beds capped by slightly coarser-grained compacted sandstone layers, which have eroded into bench-like ledges (Figure 2). These layers occur with some regularity throughout the stratigraphy, and so were ascribed numbers in previous expeditions, beginning with number one pertaining to the most basal bench at the bottom of the formation and progressing upward through “Bench 19”, which is the top-most of the ledge-forming layers. Thus far, pterosaur material has been preserved and recovered from the finer-grained layer above Bench 19, which is abundantly fossiliferous (Figure 2). In fact, most vertebrate specimens recovered by Projecto PaleoAngola have been found concentrated in a 1–2 m thick interval directly overlying Bench 19 [28]. This upper portion is capped by about 10 m of fine-grained sandstone, the base of which is characterized by pale yellow to white fine-grained and weakly cemented sediments, which grade to a darker, coarser yellow silty sand within the first few meters. Most of the pterosaur material was found in this unit.

Based on the paleogeography of the Bentiaba region's coastline, Bench 19 was deposited on a narrow, shallow marine shelf along the shoreline at approximately 24° S paleolatitude in waters between 50 and 100 m in depth and with a paleotemperature of 18 °C based on the  $\delta^{18}\text{O}$  from the bivalve shells [26,28,29]. Based on the fossil assemblage, this was a highly productive marine environment characterized by relatively low sedimentation rates compared to bone input [28]. The manner in which the fossils are interspersed throughout the layer implies general taphonomic scattering over the sea floor because there is very little erosion or signs of transport on the bone surfaces and the bones are in fairly pristine condition [28]. Disarticulation of the skeletons may have been due to scavenging, as is evidenced by the visible bite marks and scratches that are found on certain bones retrieved from the locality [28], a premise which is supported by the abundant shed shark and other predatory teeth that have been recovered from the surrounding matrix of the same locality.

## 5. Description

The total number of pterosaur specimens collected consists of possibly 11 Individuals including 14 elements, all of which were collected from the same stratigraphic layer (Table 1). The hollowness and pneumatization of these particular bones, by elimination, points to the fact that they are representative of either a member of the Theropoda (including Aves) or Pterosauria [30–33]. Additionally, following the typical criteria for the Pterosauria [31], all of the Angola specimens have very thin cortical bone, varying in thickness between 0.3 to 1.6 mm. All of the fossils preserve their three-dimensionality, although the cortical bone surfaces are superficially fractured overall on all of the specimens, likely due to lithostatic pressure. All of the following descriptions of wing elements are oriented as they would be in flight, with the humerus and antebrachium are discussed as though the long axes of their cross-sections are vertical, and the leg elements are oriented in a standing position. All diagnostic material is fully described herein. See Supporting Information S3 for full descriptions of additional fragmentary material that is only referable to the Pterosauria or the Pterodactyloidea.

**Table 1.** Bentiaba pterosaur elements and attributions.

Specimen Number	Material	Taxonomic Identification
MGUAN-PA163	Left Femur	Pteranodontia
MGUAN-PA650	Left Humerus fragment (distal) & Left Ulna	<i>Epapatelo otyikokolo</i> , Gen. et sp. nov.
MGUAN-PA652	Left Manual Digit IV Phalanx 3 fragment (proximal)	Pterosauria
MGUAN-PA653	Right Ulna fragment (distal)	Pterosauria
MGUAN-PA654	Right Metacarpal IV fragment (distal) & Right Manual Digit IV Phalanx 1 fragment (proximal)	Pteranodontia
MGUAN-PA656	Left Manual Digit IV Phalanx 2 fragment (distal)	Pterosauria
MGUAN-PA657	Left Manual Digit IV Phalanx 1 fragment (proximal)	Pterosauria
MGUAN-PA658	Shaft fragment	Pterosauria
MGUAN-PA659	Left Manual Digit IV phalanx 1	Pterosauria
MGUAN-PA660	Right Metacarpal IV fragment (proximal)	Pterodactyloidea
MGUAN-PA661	Left Ulna & Left Radius	<i>Epapatelo otyikokolo</i> , Gen. et sp. nov.

### 5.1. *Epapatelo otyikokolo*, Gen. et sp. Nov

#### 5.1.1. MGUAN-PA650 Humerus

MGUAN-PA650 (Figure 3) is a left humerus fragment comprising a partial shaft through the distal end (found in situ articulated with an ulna). The humerus bone surface is crushed inward for a section of the shaft on the posterior surface, although it retains its

original three-dimensional shape at its distal-most end. The anterior and posterior condyles are damaged and are largely missing.

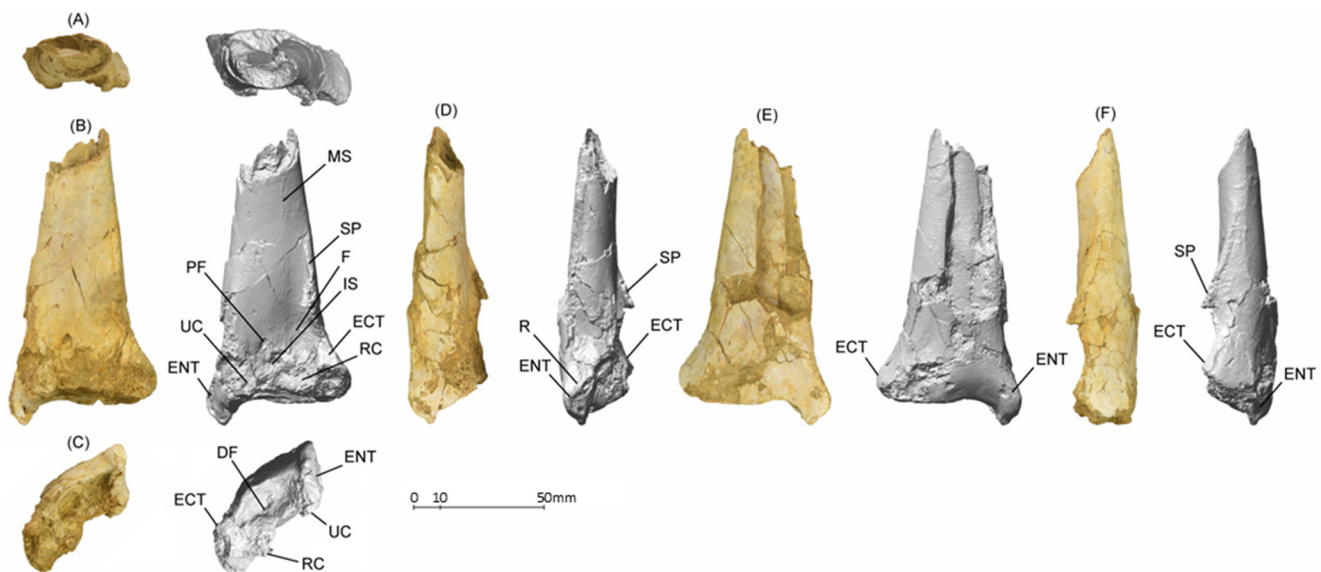


**Figure 3.** Holotype MGUAN-PA650 *Epatatelo otyikokolo*, gen. et sp. Nov. left humerus fragment. Photographs and surface scans in (A) proximal, (B) anterior, (C) distal, (D) ventral, (E) posterior, and (F) dorsal views. Abbreviations: DF, distal fossa; ECT, ectepicondyle; ENT, entepicondyle; F, fossa; IS, intercondylar sulcus; MS, muscle scar; PF, pneumatic foramen; R, ridge; RC, radial condyle SP, supracondylar process; UC, ulnar condyle.

Dorsoventrally, the bone is relatively planar and is expanded distally. Anteroposteriorly, the shaft expands gradually toward the distal margin of the condylar area in a distinct bell-shaped flare. The shaft is elliptical in its cross-section. The proximodistal length of the fragment measures 108.3 mm in length, yielding an estimated total length at about 212 mm (estimation methodology discussed further in wingspan calculation). Dorsoventrally, the humerus is 57.6 mm at the widest part of its distal end and 24.9 mm at the narrowest part of the shaft, making the distal end well over twice the minimum width of the remaining preserved shaft. The anteroposterior mid-depth measures 15.7 mm at the narrowest end of the shaft and 24.3 mm at the distal end. The cortical bone ranges from 0.5 mm to 1.4 mm in thickness. The supracondylar process is a thin prominent crest running along the anterodorsal edge of the shaft, beginning 64.5 mm from the distal end of the ectepicondyle, reaching its apex at 36.9 mm from the end, and gradually diminishing toward the ectepicondyle. Ventrally bordering the supracondylar process and proximal to the dorsal condyle lies the shallow triangular fossa. The shaft of the humerus bears a slightly raised and thin longitudinal scar on the anterior surface close to its dorsal edge that is likely the origin of the brachialis muscle [32].

The entepicondyle is elongated and is 18.6 mm in proximodistal length and 10.6 mm in dorsoventral width. The ectepicondyle, which is 14.4 mm in proximodistal length and 16.3 mm in dorsoventral width, is rounded in the horizontal outline. The entepicondyle expands prominently ventrodistally from the posterior condyle, which is either missing the portions formed by the distal epiphyses sensu Bennett [33] or is somewhat eroded. The posterior surface of the entepicondyle bulges to form a posteroventral ridge, sloping towards a tapered distal point. In contrast, the ectepicondyle projects dorsally and slightly anteriorly from the dorsal condyle. On the anterior surface, a 4.9 mm-long by 2.7 mm-wide elliptical pneumatic foramen is clearly visible proximal to the dorsal and ventral condyles at the proximal end of the intercondylar sulcus, slightly closer to the ventral condyle. The proximal margin of the foramen is deeper and well-defined, but the distinct margin diminishes as the foramen becomes shallower distally. Rugosities are visible on the ventral

surface of the shaft proximal to the entepicondyle and are the origin for the carpus and digit extensors [32] as well as on the dorsal surface of the shaft proximal to the ectepicondyle, representing the origin of the lateral head of the triceps [32].

Distally, the entepicondyle forms a ventrodistally elongated projection, which is distally flattened on the posterior surface and is acute distally. In contrast, the ectepicondyle forms a broad subtriangular outline, which is flattened distally. Posterior to the condyles on the distal surface lies a dorsoventrally oriented figure eight-shaped distal fossa. The distal fossa is positioned more ventrally and is halved by a shallow prominence. The anterior margin of the fossa is partially eroded. The posterior margin of the fossa is sinusoidal, dorsally more concave, and ventrally more convex. The surface of the distal fossa is dotted with small circular pits, some more elongated than others, implying an incompletely ossified distal end and therefore an osteologically immature individual. Two ovoid pits in the distal fossa separated by the shallow prominence are articulation surfaces for the epiphyseal cartilage.

### 5.1.2. MGUAN-PA650 Ulna

MGUAN-PA650 (Figure 4) is a left ulna, which was found articulated in situ with humerus fragment MGUAN-PA650. It is very nearly complete, save for a few sections of missing cortical bone on the olecranon process, the dorsal surface of the proximal shaft, and on both the dorsal and ventral distal terminal expansions, which are partially eroded. Sediment infill in those missing regions retains the bone's three-dimensionality.

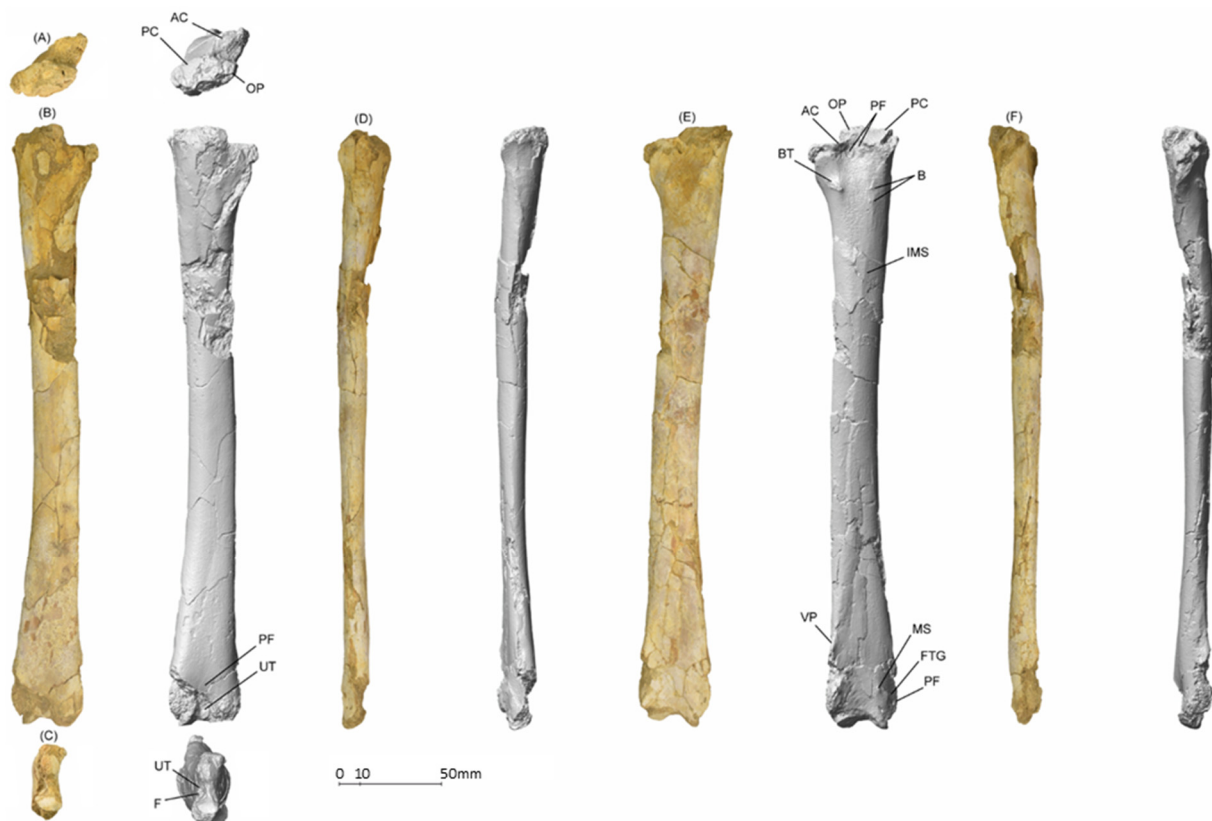


**Figure 4.** Holotype MGUAN-PA650 *Epapatelo otyikokolo*, gen. et sp. nov. left ulna. (A) proximal, (B) posterior, (C) distal, (D) dorsal, (E) anterior, and (F) ventral views. Abbreviations: AC, anterior cotyle; B, bump; BT, biceps tubercle; F, fovea; FTG, flexor tendon groove; MS, muscle scar; OP, olecranon process; PC, posterior cotyle; PF, pneumatic foramen; and UT, ulnar tubercle; IMS, interosseous membrane scar; VP, ventral process.

The ulna is elongated and straight. In the transverse plane, the proximal and distal ends expand slightly outward from the shaft. The ulna measures 290.1 mm in total length, and has a dorsoventral width of 44.1 mm at the widest point of the proximal end, 21.3 mm at the narrowest point of the shaft (22.4 mm at the midpoint of the shaft), and 35.3 mm at the widest point of the distal end. The cortical bone ranges from about 0.5 mm to 1.6 mm in thickness. The shaft is anteroposteriorly flattened and elliptical in its cross-section. Anteroposteriorly, the breadth of the shaft measures 11.8 mm at its narrowest point, 18.2 mm at the broadest proximal end, and 14.1 mm at the broadest part of the distal end. The shaft's anterior surface exhibits a faintly raised longitudinal ridge, the interosseus membrane scar of Bennett [33], which is dorsally offset at the proximal end and extends gradually towards the center of the shaft for along most of the proximal half of the ulna. At the proximal end of the ulna, two elliptical foramina are evident on the shaft's anterior surface, distal to the overlap of dorsal and ventral cotyles. The larger foramen measures 4.9 mm in proximodistal length and 2.8 mm in dorsoventral width and lies dorsal to the smaller one, which measures 1.8 mm in length and 1.2 mm in width. The biceps tubercle is ventrally offset, distal to the ventral cotyle, and is a slightly anterodistally elongated rugose protuberance that is 9.7 mm in length. Dorsal to the biceps tubercle and distal to the anterior cotyle lie two significantly smaller tubercles, the anchor for the radioulnar ligament of Bennett [33]. The more proximal bump distally borders a small rugose area on the shaft surface. The posterior surface of the ulnar shaft is relatively featureless.

In the transverse plane, the proximal articular area of the ulna is asymmetrical. The ventral expansion is oriented ventrally and slightly anteriorly away from the shaft and is capped proximally by the ventral cotyle, whereas the dorsal side exhibits hardly any expansion apart from a slight anterior curvature. The proximal end of the ulna is kidney-shaped in the cross-section, with concavity on the anterior side, whereas the shaft is elliptical in the cross-section. The olecranon process is slightly eroded. A small intercotylar crest divides the articular surfaces. The dorsal cotyle is saddle-shaped (concave anteroposteriorly and convex dorsoventrally) with a gentle anteroproximal tilt. The dorsal cotyle is more proximally placed than the ventral cotyle, forming a step between the articular surfaces. The dorsal cotyle is anteroposteriorly concave.

On the distal end of the ulna, the beginning of the ventral expansion is preserved as a slight process, forming a ridge 44.8 mm from the distal edge, although much of the distal portion of the process has been eroded. In anterior view, the flexor tendon groove lies on the dorsal side of the shaft, with an apparent nutrient foramen located dorsal to it. On the ventral margin of the groove is a rugose ridge, which exhibits as a raised tubercle with a muscle scar. On the posterior surface, a large pneumatic foramen measuring 9.3 mm in length and 3.6 mm in width lies between and proximal to the distal articular surfaces.

On the distal surface, two distinct articular surfaces of the proximal syncarpal lie in a row in a figure eight-shaped configuration, with the distal tuberculum slightly ventrally in between. The surfaces are partially eroded to the point that trabecular bone is visible. What remains of the rounded dorsal articular surface is anteroposteriorly expanded from the shaft and oriented posterodistally, with the fovea located on its posterior side. The distal tuberculum lies ventral to the dorsal articular surface, is projected dorsoventrally from the center point of the distal end of the ulna, and is inclined proximovertrally.

### 5.1.3. MGUAN-PA661 Ulna and Radius

MGUAN-PA661 is a nearly complete left ulna and was found in articulation with the radius (Figure 5). The ulna measures 341.0 mm in proximodistal length, 62.3 mm in dorsoventral width at the widest part of the proximal end, 34.3 mm in dorsoventral width at the midpoint of the shaft, 53.3 mm in dorsoventral width at the distal end, 9.3 mm in anteroposterior breadth at the broken distal end of the shaft, and 19.7 mm in anteroposterior breadth at the widest part of the proximal articular end. The bone ranges from 0.5 mm to 1.0 mm in cortical thickness. It is fairly well-preserved, with an intact three-dimensional shape. The cortical bone shows no loss of bone surface, except for at the proximal and

distal ends, with the distal ends being significantly eroded, making the features difficult to discern. At the proximal end of the ulna, an elliptical foramen is barely visible on the shaft's anterior surface, distal to the overlap of the dorsal and ventral cotyles. In distal view, the shaft is elliptical in the cross-section and is slightly compressed anteroposteriorly. The ulna is elongated and straight, and the shaft exhibits a faintly raised longitudinal ridge, the interosseus membrane scar, which appears to run parallel to and dorsally offset from the midline of the shaft, gradually migrating more towards the midline distally for as long as it can be distinguished.

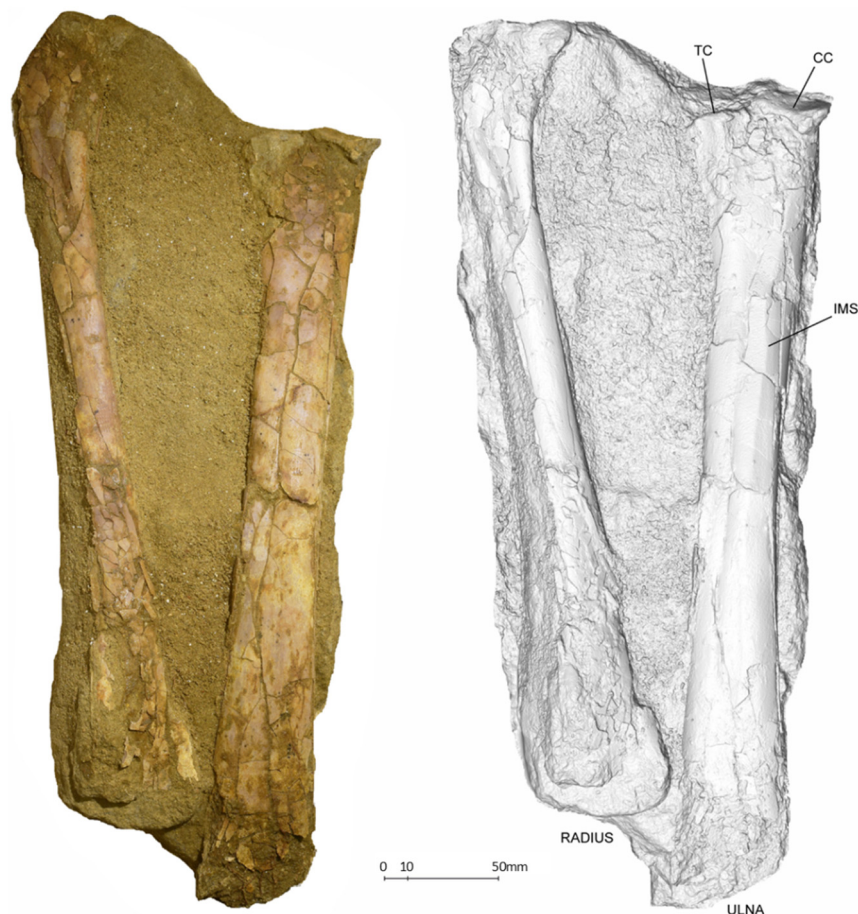


**Figure 5.** Paratype MGUAN-PA661 *Epapatelo otyikokolo* gen. et sp. nov. left ulna and left radius. In anterior view. Abbreviations: CC, dorsal cotyle; TC, ventral cotyle; IMS, interosseous membrane scar.

In anterior view, the shaft expands slightly dorsoventrally from the center of the shaft as it approaches both articular ends. At the proximal end, the dorsal cotyle manifests as a concave crescentic articular surface, spanning just over half of the dorsoventral width of the ulna from beyond the dorsal point of the shaft to just past the midline of the shaft and is angled at a slight ventroproximal tilt. The ventral cotyle occupies the remainder of the proximal surface of the ulna and is slightly dorsoventrally concave.

The shaft of the radius, MGUAN-PA661, is relatively straight and elliptical in the cross-section. The shaft expands dorsoventrally as it approaches both articular ends. It measures 332.0 mm in proximodistal length, 30.4 mm in dorsoventral width at the proximal end, 19.1 mm in dorsoventral width at the midpoint of the shaft, 52.1 mm in dorsoventral width at the distal end of the preserved shaft, 7.1 mm in anteroposterior breadth at the proximal end, and 14.8 mm in anteroposterior breadth at the distal end of the shaft. The cortical bone ranges from 0.4 mm to 1.0 mm in thickness. Although it maintains its three-dimensional

shape, it is highly eroded, particularly around the proximal and the distal articular surfaces, making it difficult to distinguish features.

## 5.2. *Pteranodontia* Indet MGUAN-PA163 Femur

MGUAN-PA163 (Figure 6) is a relatively complete left femur [10] and is lacking the greater trochanter, the distal condyles, and a few sections of cortical bone at the distal end on the lateral and anterior sides of the shaft, with a sediment interior mold preserving the original shape. The femoral head is lightly eroded, revealing the trabecular bone, and damage is evident around the base of the neck. Cortical bone ranges from about 0.4 mm to 0.7 mm in thickness.



**Figure 6.** MGUAN-PA163 left femur. (A) proximal, (B) anterior, (C) distal, (D) medial, (E) posterior, and (F) lateral views. Abbreviations: FT, fourth trochanter scar; IT, internal trochanter; MS, muscle scar; PF, pneumatic foramina; POF, popliteal fossa.

The proximodistal preserved length of the femur is 155.8 mm. The narrowest part of the shaft is in the upper third, where it measures 11.2 mm in mediolateral width, with the width steadily increasing distally to 12.8 mm at the midpoint of the femur. It is almost double its mediolateral width, which measures 18.8 mm at the distal end. In lateral view, the femur has a minimum anteroposterior breadth of 10.9 mm, the narrowest part occurring halfway down the shaft. It is 12.4 mm in anteroposterior breadth at the widest part of the proximal shaft and 11.9 mm in anteroposterior breadth at the widest part of the complete distal shaft.

The femoral head is bulbous and rounded, projecting proximomedially from a long, constricted neck that exhibits a slight anterior curvature and positioned at a  $146^\circ$  angle to the shaft. Although most of the greater trochanter and the internal trochanter are eroded away, they are conspicuous at the margins of the shaft bordering these areas, which are distinctly sloped. Trabecular bone is visible along the broken margins of the trochanters. In proximal view, a mediolaterally oriented lenticular pneumatic foramen is sunken into the large concave ventral intertrochanteric fossa. The length of the femoral neck, from the intertrochlear fossa to the head, is 16.5 mm, and the neck has a circular cross-section.

In the transverse plane, the shaft of the femur is bowed posterolaterally, exhibiting a gradual curve. In the cross-section, the shaft is circular at the base of the trochanters and expands distally, gradually becoming more subtriangular and twisting slightly as it approaches the distal end.

In posterior view, the internal trochanter is visible as a slightly raised ridge distal to the proximal end and centered on the shaft. Distal to this scar, the fourth trochanter scar presents as a rugosity at the distal end of the adductor ridge, which is located centrally and extends distally for approximately 60.5 mm down the length of the shaft, terminating at 23.6 mm from the distal end. Distal to the limit of the fourth trochanter scar the beginning of a slight depression can be observed, which is the beginning of the popliteal fossa.

The distal condyles are completely eroded away. In distal view an interior sedimentary mold exhibits a reinforced shape that is posteriorly concave and anteriorly convex toward the area of the intercondylar sulcus.

### 5.3. *Pteranodontoidea* Indet

#### 5.3.1. MGUAN-PA654 Metacarpal IV

MGUAN-PA654 (Figure 7) is a right metacarpal IV fragment composed of a distal shaft and articular surface (articulated with a right manual digit IV phalanx 1). The metacarpal measures 65.3 mm in proximodistal length, 17.1 mm in dorsoventral width at the narrowest part of the shaft, and 18.5 mm in dorsoventral width at the widest part of the condylar area. In the horizontal plane, it measures 11.6 mm in anteroposterior breadth at the narrowest part of the shaft and 20.7 mm in anteroposterior breadth at the widest part of the condylar area. The cortical bone ranges from about 0.6 mm to 1.1 mm in thickness. It is robust and well-preserved. The fragment shows no significant loss of bone surface, is virtually uncrushed, and is three-dimensional. The shaft is straight and flattened anteroposteriorly, with a rounded rectangular cross-section.

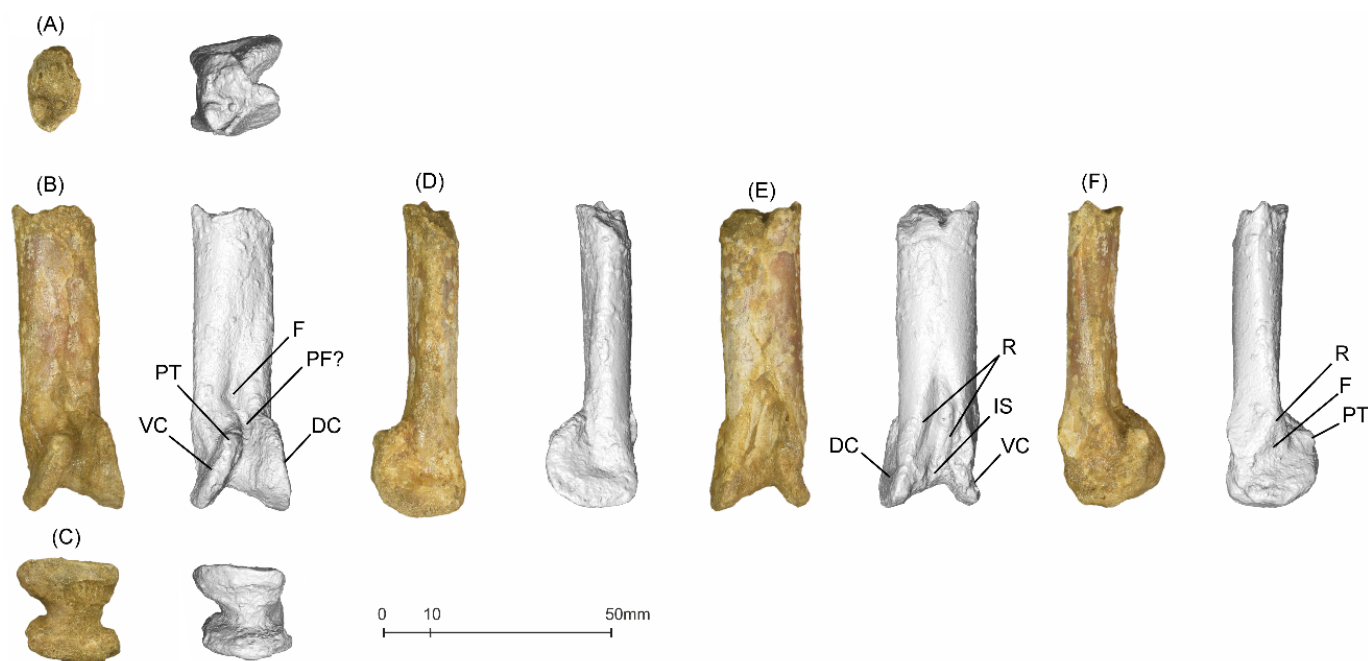


**Figure 7.** MGUAN-PA654 right metacarpal IV fragment. (A) proximal, (B) posterior, (C) distal, (D) dorsal, (E) anterior, and (F) ventral views. Abbreviations: DC, dorsal condyle; F, fossa; IS, intercondylar sulcus; PF, pneumatic foramen; PT, posterior tubercle; R, ridge; VC, ventral condyle.

In the transverse plane, the distal condylar area is deflected dorsally at a 12.1 mm offset from the center of the shaft, and the condyles have a 6° condylar skew from each other. Centered on the shaft and about 28.4 mm from the distal end, a V-shaped inter-

condylar sulcus expands distally, becoming the central concavity between the condyles. Proximally, the dorsal and ventral borders of this depression manifest as slight ridges, which converge with the distal condyles. The condylar area forms a pulley-like shape, with the ventral condyle having a ventrodorsal orientation and the dorsal condyle being oriented dorsodistally to a lesser degree.

On the ventral surface, as the shaft approaches the condylar area, a slight ridge on the posterior side buttresses the condyle and tapers to meet the triangular ventrodorsally oriented fossa. From this point of convergence, the condyle splays distally and posteriorly into a fan-like, crescentic projection, terminating with a posterior tubercle. Unlike the dorsal surface of the shaft, the ventral surface of the shaft remains straight until its abrupt intersection with the lunate ventral condyle, which also projects distally and posteriorly.

In posterior view, a proximodistally oriented lenticular fossa is positioned proximal to the pulley-shaped condylar area on the central shaft. Distal to this fossa and between the bases of the condyles is a pneumatic foramen, although sediment infilling makes this difficult to determine conclusively. The distal intercondylar sulcus is asymmetrical, with the deepest part of the concavity occurring ventrally.

In distal view, the condylar area forms a vertically oriented hourglass shape, and as the central constriction occurs slightly ventrally, the ventral condyle is slenderer than the dorsal condyle.

### 5.3.2. MGUAN-PA654 Manual Digit IV Phalanx 1

MGUAN-PA654 (Figure 8) is a right manual digit IV phalanx 1 that consists of a proximal articular end and shaft fragment. The fragment measures 215.1 mm in preserved proximodistal length (including the extensor tendon process), 42.2 mm in anteroposterior width at the widest part of the proximal end, and 18.4 mm in anteroposterior width at the distal end of the shaft. It is 8.7 mm in dorsoventral height at the broken end of the shaft, and 16.1 mm in dorsoventral height at the deepest part of the articular end. The extensor tendon process measures 11.4 mm in width at its base, and 15.5 mm in height. The cortical bone ranges from 0.3 mm to 0.7 mm in thickness. It is relatively well-preserved, with an intact three-dimensional shape. There is no significant loss of cortical bone surface. The extensor tendon process is fully fused to the phalanx on its proximal end, which indicates skeletal maturity [34]. The preserved shaft is broken and flexed dorsally and slightly anteriorly at its preserved midpoint, which imparts a slightly V-shaped form, whereas undeformed, it would have been straight. In distal view, the broken end of the shaft is elliptical in the cross-section and is flattened dorsoventrally. In ventral view, the distal two-thirds of the preserved bone has not been prepared from the surrounding matrix.

In the horizontal outline, the shaft expands posteriorly and slightly anteriorly as it approaches the proximal end. In ventral view, the ventral cotyle manifests at the proximal end of the phalanx as a concave crescent from the midline of the shaft to the tip of the extensor tendon process, forming an articular facet. The extensor tendon process projects proximally and is sub-rectangular in the horizontal outline, with a constriction at its base. At this constriction, on its posterior surface and dorsal to the ventral cotyle lies a lenticular foramen. On the anterior edge of the extensor tendon process, a convex protuberance rises anterodorsally.

Dorsally, the posterior side of the articular end is delineated by the posterior tip of the dorsal cotyle. Anterior to this cotyle, the phalanx shaft is bisected by the ventral cotyle, the distal end of which projects posteroventrally from the central region of the shaft. From there, the dorsal border of the ventral cotyle contacts with the ventral border of the dorsal cotyle, merging upward into a ridge. The ventral border of the ventral cotyle also manifests as a sharp longitudinal ridge extending down the shaft.

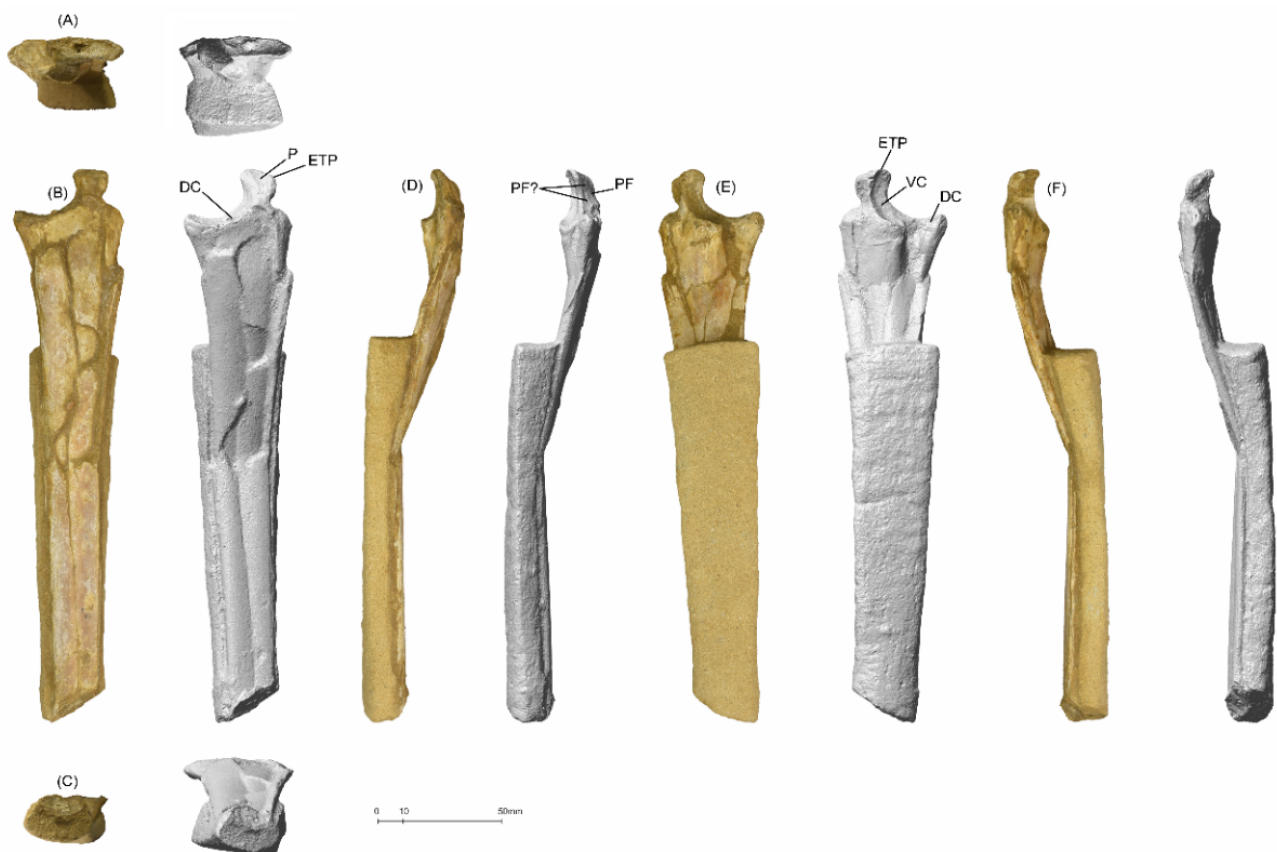


**Figure 8.** MGUAN-PA654 right manual digit IV phalanx 1 fragment. (A) proximal, (B) dorsal, (C) distal, (D) posterior, (E) ventral, and (F) anterior views. Abbreviations: DC, dorsal cotyle; ETP, extensor tendon process; P, protuberance; PF, pneumatic foramen; VC, ventral cotyle.

In proximal view, the bicotylar ginglymus at the end of the phalanx is bisected by an intercotylar ridge. This ridge originates at the anteroventral point of the dorsal cotyle, flanks the junction created by the meeting of both cotyles, and terminates proximally on the margin of the extensor tendon process. The dorsal cotyle spans the posterior half of the phalanx, excluding the area of the extensor tendon process. The ventral cotyle is positioned on the midline and is half the anteroposterior span of the dorsal cotyle and teardrop in outline, with a reduction in width occurring proximally as it reaches the extensor tendon process. In this view, the extensor tendon process is subrectangular in the outline, with the widest side directed anterodorsally.

## 6. Additional Material

Additional pterosaur material remains both in situ in Bentiaba as well as in storage in Angola. Worthy particular mention is a partial manual digit IV metacarpal fragment articulated with a first phalanx fragment, which measures at least 830 mm. This indicates extreme size variation among the pterosaurs of this region.

A few other isolated bone fragments were recovered from Bentiaba, but these shards are too shattered and indeterminate to add descriptive or diagnostic value to this work. However, they retain inherent value for future histological studies or destructive testing and for future analytical advances; therefore, their existence is mentioned here.

## 7. Results

### 7.1. Systematic Paleontology

**Pterosauria** Owen, 1842 [35,36].

**Pterodactyloidea** Plieninger, 1901 [37,38].

**Pteranodontia** Marsh, 1876 [30] sensu Unwin [39].

***Epapatelo otyikokolo*** gen. et sp. nov.

**Etymology:** The genus name “*Epapatelo*” is the translation of the word from the Nhaneca dialect meaning “wing”, and the meaning of the species name “*otyikokolo*” is the translation of “lizard” [40]. The Nhaneca (Nyaneka) are the indigenous nomadic group who originate in Angola’s Namibe Province (the region of the fossils’ locality).

**Holotype:** The holotype is the distal half of a left humerus MGUAN-PA650 articulated with a left ulna MGUAN-PA650 from a single individual.

**Paratype:** The paratype is an articulated left ulna and left radius MGUAN-PA661, taken from a single individual.

**Type locality:** Region to the north of the Bentiaba River, near the commune of Bentiaba, Moçâmedes Municipality, Namibe Province, Angola. Approximate coordinates are 14.2° S, 12.3° E. Paleolatitude during the Maastrichtian: near 24° S [26,41].

**Type horizon:** Upper portion of the Mucuío Formation (Figure 3). Lower Maastrichtian (71.64–71.40 Ma), Upper Cretaceous.

**Diagnosis:** Pteranodontian with a flared bell-shaped distal expansion of the humerus; humerus ectepicondyle with a prominent dorsal projection; sharp narrow lamina on the dorsodistal margin of humerus and distal fossa that borders most of the distal face; step-like distal position of the ventral cotyle from the dorsal cotyle on the proximal ulna; and a ventrally positioned distal tuberculum on the ulna.

**Aponyctosauria/Aponyctosauria** New Clade

**Definition:** Most inclusive clade exhibiting a hatchet-shaped deltopectoral crest of the humerus, synapomorphic with that in *Nyctosaurus gracilis* Marsh, 1876 [30].

**Composition:** The Nyctosauridae, *Alcione elainus*, *Simurghia robusta*, and *Epapatelo otyikokolo*.

### 7.2. Phylogenetic Analysis

Phylogenetic analysis was conducted for the combined *Epapatelo otyikokolo* holotype and paratype (MGUAN-PA650 and MGUAN-PA661) and other named Pterosauria. The analysis resulted in four equally parsimonious trees (Figure 9). These trees are the result of four phylogenetic positions for *Volgadraco bogolubovi* Averianov et al. 2008 [42] (a rogue taxon in Longrich et al. 2018 [17]) with *V. bogolubovi* recovered in a trichotomy with *Alamodactylus byrdi* Andres & Myers 2013 [43] and for all of the other pteranodontians that are more closely related to *Nyctosaurus*; in a tetranomy with *Simurghia robusta* Longrich et al. 2018 [17], *Alcione elainus* Longrich et al. 2018 [17], and the Angola specimens; in a trichotomy with these taxa and the Nyctosauridae; and in a trichotomy with *C. hlavaci* and all of the pteranodontians that are more closely related to *Nyctosaurus* than *A. byrdi*. The phylogenetic placement of *V. bogolubovi* has no specific bearing on the relationships of the Angola specimen, so it can be safely deactivated (i.e., with the taxcode command) to highlight the relationships of *E. otyikokolo*. When *V. bogolubovi* is excluded, there is one tree that is more parsimonious than the rest. *Epapatelo otyikokolo* is recovered in a trichotomy with *S. robusta* and *A. elainus* in the Pteranodontia. The Nyctosauridae was phylogenetically defined as the least inclusive group, including *Muzquizopteryx coahuilensis* Frey et al. 2006 [44] and *Nyctosaurus gracilis* Marsh, 1876 [30] by Andres et al. 2014 [18], and under this definition, the clade that includes *E. otyikokolo*, *S. robusta* and *A. elainus* is a sister group to the Nyctosauridae. *Epapatelo otyikokolo* is a non-nyctosaurid pteranodontian.

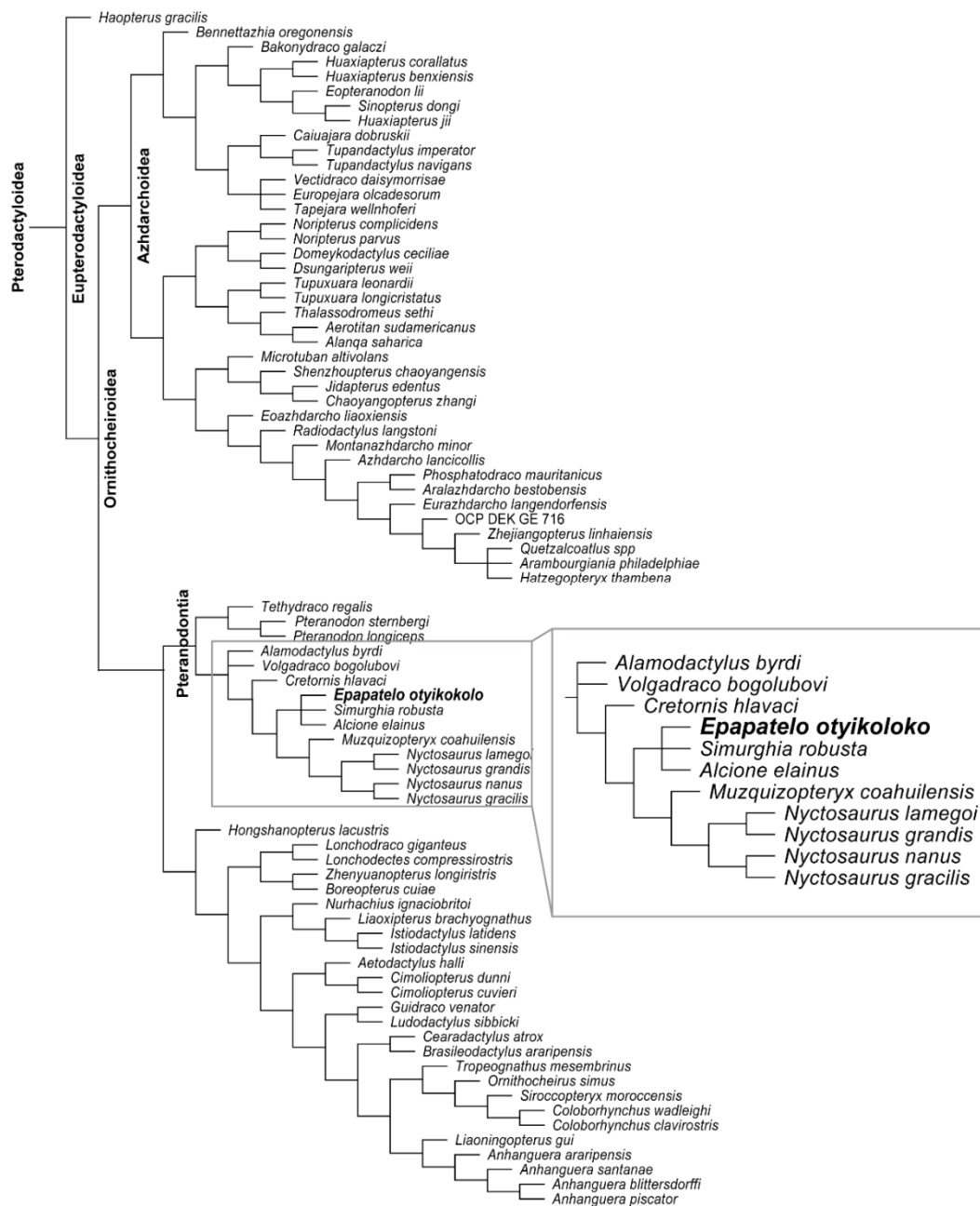


**Figure 9. Adams consensus cladogram.** Based on the four resultant equally parsimonious trees from the phylogenetic analysis of Longrich et al. 2018 [17] with the addition of *Epapatelo otyikokolo*, gen. et sp. nov. (articulated humerus and ulna, with articulated radius and ulna). These trees differ only in their placement of *Volgadraco bogolubovi* Averianov et al. 2008 [42], which is shown at its most basal position recovered.

### 7.3. Wingspan Calculation

The size estimation technique used to calculate the total wingspan of *E. otyikokolo* relies on the phylogenetic reconstruction method of Andres et al. 2014 [18] and was performed with the phylogenetic analysis presented here. The continuous data partition code ratios of all major wing element lengths are such that if an element is missing in a taxon, the ratio of it to other elements can be estimated on the cladogram for that taxon using ancestral state reconstruction. It should be noted that the tree(s) from the analysis should be saved and loaded without rescaling any of the characters (i.e., without the ‘nstates stand’ command). With the ratios of all major limb elements estimated, it just requires a single

complete bone length to calculate the total wingspan. In this case, the complete ulna length of MPUAN-PA650 can be used to calculate the humerus length using character 30, the resultant humerus estimate can be used to estimate the length of the wing metacarpal using character 33 and the length of the first wing phalanx using character 36, and the resultant first wing phalanx estimate can then be used to calculate the length of the second through fourth wing phalanges using characters 37–39. The total wingspan estimate is calculated using the method of Bennett [45], wherein the humerus, ulna, wing metacarpal, and wing phalanges are summed. The omission of orientation and the flexures of the bones is meant to compensate for not including the trunk and carpus of pterosaurs. Each wing is found to measure just over 2.4 m, giving *E. otyikokolo* approximately a 4.8 m wingspan (Table 2). In order to determine an overall body size of the specimens, the lengths of the incomplete wing elements were calculated based on the length of the complete ulna, MGUAN-PA650. This produces an average estimate for the MGUAN-PA650 humerus at 213.5 mm, plausibly indicating that just over half of the humerus is preserved in MGUAN-PA650.

**Table 2.** *Epapatelo otyikokolo*, gen. et sp. nov. MGUAN-PA650-calculated humerus length and known MGUAN-PA650 ulna length measurements, with estimated additional individual wing element lengths.

Element	Length
Humerus	213.5 mm (estimated)
Ulna	290.1 mm
Metacarpal IV	459.8 mm (estimated)
Digit IV Phalanx I	518.3 mm (estimated)
Digit IV Phalanx II	421.9 mm (estimated)
Digit IV Phalanx III	307.4 mm (estimated)
Digit IV Phalanx IV	153.9 mm (estimated)
<b>Estimated Individual Wing Length = 2.4 m</b>	
<b>Total Estimated Wingspan = 4.8 m</b>	

These dimensional proportions can then also be scaled up and down and used to produce size estimates of other individuals of the same species with complete bones, giving the articulated MGUAN-PA661 ulna and radius a 5.6 m wingspan. However, the existence of other further size-variable individuals in the fossil assemblage, namely the much larger MGUAN-PA653 ulna (and an extraordinarily large unnumbered specimen referred to earlier in this work), indicate that there was an even wider size variability in the group than we find here. This overall variability exceeds the fluctuating size variation and could be reasonably attributed to sexual dimorphism (as observed in known reptiles [46]), or even just to intraspecific or ontogenetic variation, and therefore, it is most likely that the assemblage represents several different species, which, in the current absence of more concrete diagnostic material, could henceforth only be definitively clarified by conducting further field sampling.

#### 7.4. Bone Histology

Interpreting the ontogenetic stage of a fossil taxon is traditionally reliant on the degree of fusion of the bones or degree of ossification of the cartilage (both in the epiphyseal regions and between elements), the extent of ossification, surface textures, and histology [34,47]. No traces of sutures were found on the distal end of humerus MGUAN-PA650, fusion of the extensor tendon process on all first wing phalanges present in the assemblage appears to be fully completed, and no immature grain on the limb bone shafts was observed. Therefore, in order to further explore the ontogenetic variability in the Angolan fossil assemblage, histology was relied upon to infer the ontogenetic stage and growth rate based on growth rings, vascularization patterns, and the organization of the collagen fibers [48,49]. In pterosaurs, identifying histological features is complex compared to in other tetrapods because they have the thinnest cortical bone walls [48], which retain a sparse record of their growth dynamics. Considering that pterosaur bone tissue is quickly reabsorbed by

osteoclasts from the inner medullary cavity as they grow outwardly, the primary bone structure disappears rapidly, as do any lines of arrested growth (LAG) that may have been previously formed [50]. A 0.6 mm-thick fragment of the MGUAN-PA653 ulna was chosen as the sample for histological analysis because long bones undergo the least metaplastic deformation throughout growth [51]. Ulnae are of particular interest in flying vertebrates because they are the main supporting bone of the zeugopodium that bears the brunt of the flight load on the wing and are especially subject to torsional forces. They endure a great amount of shearing stress at the tissue level, and they compensate by having the highest laminarity of all bones [52,53].

The MGUAN-PA653 ulna is composed of a cortical layer with a periosteum composed of mature bone with a plywood-like pattern (Figure 10). Under cross-polarized light, which reveals the original orientation of collagen fibers, bone cells manifest as a spindle shape, which then orient themselves according to the orientation of the ply [49]. This is visible here as the fibers alternate in orientation, from longitudinal to circumferential, and can also be seen as alternating colors under crossed polarized light with a lambda filter (Figure 11). This type of poorly vascularized parallel-fibered bone indicates an advanced arrangement of the tissue, which specifies that the sample is post-juvenile.

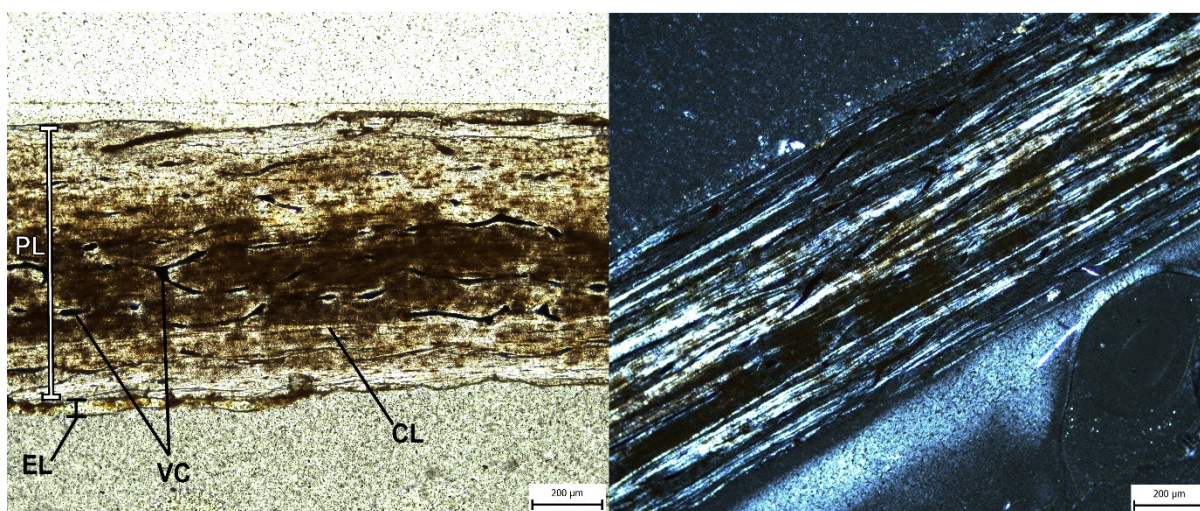


**Figure 10.** Thin section of MGUAN-PA653 ulna fragment under normal light (**left**) and cross-polarized light (**right**). Abbreviations: CL, circumferential lamella; EL, endosteal layer; PL, periosteal layer; VC, vascular canals.

The periosteum comprises a sparse array of vascular canals and primary osteons until the poorly visible inner endosteal limit is reached. The endosteal region shows great irregularity, where bone has been previously remodeled and eroded away. There is a dense, organized network of osteocytes throughout the bone sample, visible as small simple lacunae and oriented longitudinally and circularly, which may also indicate secondary remodeling [49]. It has also been suggested that these lacunae may potentially be a detection system for bone strain and damage [54]. The tissue is moderately vascularized in a circumferential or longitudinal pattern, which is again a sign of maturity because juvenile bone is usually greatly vascularized in a reticular to lamellar pattern [49]. Approaching the innermost and outermost surfaces of the bone, this vascularization lessens, and the bone becomes denser, which is a feature of mature animals that are no longer undergoing rapid growth [49,55]. Primary osteons are oriented longitudinally and are internally ringed with lamellar bone, which is visible under rotation with a lambda filter (Figure 11), and are also sometimes connected by irregular and oblique anastomoses. Secondary osteons, commonly seen in adult animals, are not visible in the sample, which could be an indication of a sub-adult age [49].

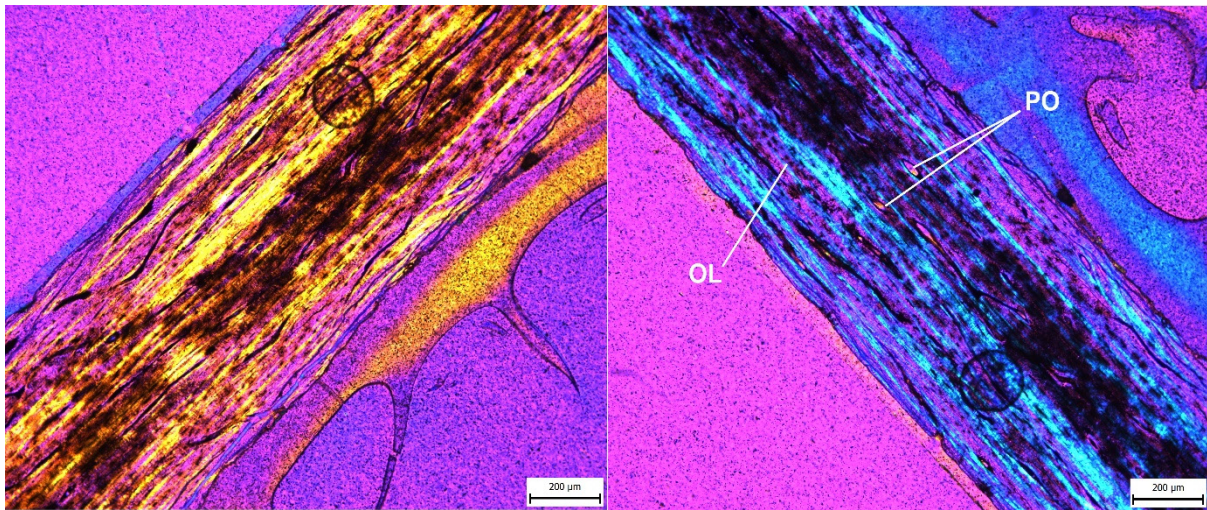


**Figure 11.** Thin section of MGUAN-PA653 ulna fragment under crossed polarized light and rotated under a lambda filter. Abbreviations: OL, osteocyte lacuna; PO, primary osteon.

In this sample, no trabeculae are visible due to this being a mid-shaft sample, which would have been especially subject to secondary reworking [56], erasing earlier records of growth. No LAGs are visible and are indeed generally uncommon in pterodactyls, although LAGs do occur in some species, including in *Pteranodon* [50,57,58]. It is also worth noting that annual growth marks do not visibly appear in vertebrates that achieve full growth in less than one year [57]. In the absence of LAGs, growth rates can be inferred by analyzing other aspects of bone type and the degree of vascularity [59]. Additionally, the presence of endosteal lamellae has been shown to be a sign of maturity in certain pterosaurs because it is a correlate for the cessation of medullary expansion [48–50,57], but although it appears that this final layer deposition may have begun in certain areas of the bone (Figure 10), any completed lamellae ringing the bone are not yet visible here either. There is also no sign of an external fundamental system, although a few vascular canals are seen to open onto the periosteal surface, which implies that the animal had not yet reached its final body size. In fact, the lack of this avascular outermost cortex implies that the animal was still growing and is the most compelling evidence for a sub-adult age.

These histological observations indicate that MGUAN-PA653 was subadult in age, not yet having reached its final determinate body size. Although histology can be an informative foray into the maturity of an individual animal, its real strength lies in relative age, especially when several samples can be taken from entire populations. Therefore, more extensive sampling of other bones in the Angolan assemblage would yield much a more informative picture of the population at that time.

### 7.5. Comparison and Discussion

*Epapatelo otyikokolo* from Bentiaba is defined by the holotype-articulated humerus and ulna (MGUAN-PA650) and is supported by a topotypic articulated ulna and radius (MGUAN-PA661). While the humerus (MGUAN-PA650) is incomplete, preserving just over half the original length, it shares a straight humeral shaft with *Tethydraco regalis*, *Alcione elainus*, and *Simurghia robusta* [17] (Figure 12). Additionally, the mid-shaft shape of the humerus expands outward as it approaches the distal end. Therefore, the isometric scaling of the humeri discussed by Longrich et al. 2018 [17], which differentiated *A. elainus* and *S. robusta* as separate species, also applies here in differentiating *Epapatelo otyikokolo* as a new species as well.



**Figure 12.** Comparison of non-nyctosaurid pteranodontian distal humeri. (A) FSAC-OB 7 *Simurghia robusta* Longrich et al. 2018 [17], (B) MGUAN-PA650 *Epatatelo otyikokolo*, and (C) FSAC-OB 5 *Alcione elainus* Longrich et al. 2018 [17].

The *Epatatelo otyikokolo* (MGUAN-PA650) humerus displays an entepicondyle that is wider than the ectepicondyle in dorsoventral width, with the ectepicondyle of the humerus projecting anteriorly (a pteranodontid feature) [17,33]. The entepicondyle projects distally, a feature shared with nyctosaur *A. elainus* [17] and azhdarchoid CMN 50814 [60] (CMN: Canadian Museum of Nature, Ottawa, Canada). This gives the humerus a strong distal expansion that is also similar to *Pteranodon* sp., *T. regalis*, and *A. elainus*, a derived feature of non-*Nyctosaurus* pteranodontoids, but different from azhdarchoids that only have an expansion of the distal one-third of the humerus [17]. In fact, the distal width of MGUAN-PA650 is more than twice the width of the narrowest part of the preserved shaft, which is a proportional feature shared with *T. regalis* [17]. MGUAN-PA650 also shares, in the distal aspect, the trapezoidal humerus shape with a relatively straight dorsal surface, which is a feature shared by pteranodontians and not azhdarchoids, which have convex posterior margins or ornithocheiromorphs that have triangular posterior margins [17,58,61]. An unusually large supracondylar process was considered an autapomorphy of *S. robusta* [17],

and although the *E. otyikokolo* humerus is too eroded to definitively assert that it shares such a feature, the edges of the process form a distinct ridge, indicating a notable expansion. In *A. elainus* and also in the *E. otyikokolo* humerus, the supracondylar process is shifted more proximally, which is a feature of these taxa and nyctosaurids. In MGUAN-PA650, distal to the supracondylar process is the hypertrophied distoventral projection from the entepicondyle, which is only shared between the *E. otyikokolo* humerus, CMN 50814, and *A. elainus*. This process shows significant muscle scarring on the dorsal surface that attaches the carpus and digit extensors [32], which may indicate a difference in function from other closely related taxa.

Appendicular pneumatic foramina are absent in basal pterosaurs. However, they are present in the Angola specimens and in gnathosaurines and are widespread in ornithocheiroids sensu Bennett [62], including *Pteranodon* [61]. These pterosaurs exhibited postcranial pneumatization by pulmonary air sacs, which gave them the lightweight and high-efficiency ventilation capabilities necessary for the strenuous active flapping [63]. The position and extent of these foramina are useful in distinguishing clades [33]. *Epapatelo otyikokolo* (MGUAN-PA650) exhibits a large ovoid pneumatic foramen ventrally and proximal to the condyles of the humerus, similar to *A. elainus*, *S. robusta* [17], and *Pteranodon* sp. [33].

With respect to the ulnae (Figure 13), the better preserved MGUAN-PA650, when compared to MGUAN-PA661, is identical in morphology, save for scaling and the fact that the MGUAN-PA650 ulna exhibits a distal tuberculum on the ventral part of the distal end, which is too eroded to be distinguished in MGUAN-PA661. The position of the distal tubercle, although more similar to azhdarchoids than pteranodontians in its placement, did not change its phylogenetic position. The proximal anterior of the surface of both ulnae are flat, similar to in other known pteranodontians, such as FSAC-OB 4, NMP Ob 10-14 (NMP: National Museum Prague, Prague, Czech Republic), and YPM 2499 and YPM 2497 (YPM: Yale Peabody Museum, New Haven, CT, USA). The distal expansions on the shafts of both known ulnae of *Epapatelo otyikokolo* are gradual, with no clear distinction between the shafts and the distal ends, similar to cf. *Tethydraco regalis* specimens FSAC-OB 199 and 200 (FSAC: Faculté des Sciences Ain Chock, Casablanca, Morocco).

Other Angolan pterosaur fossils are less determinate. The MGUAN-PA163 femur (Figure 14) was preliminarily assigned to the “Ornithocheiroidea” sensu Unwin [10,39], which corresponds to the Pteranodontoidea in this analysis, based on the femoral neck-shaft angle of  $>145^\circ$  [39]. The neck-shaft angle in the Angola femur (MGUAN-PA163) is  $146^\circ$  and lies close to the threshold, making the character difficult to code in this specimen. However, coding for this character in the matrix did not change the phylogenetic results. The MGUAN-PA163 femur also exhibits the following characteristics: a pneumatic foramen on the proximal end (found in the Ornithocheiroidea) and a constricted femoral neck shape (found in the Novialoidea). Femur shape was also difficult to code because “strongly bowed” and “slight curvature” are qualitative and difficult to distinguish from each other. However, neither character designation did not change their phylogenetic position. The Angola specimen was deemed to have a slight sigmoidal curvature in two planes, both anteroposteriorly and mediolaterally. This medial curvature is a shared trait with the Pteranodontidae and the Nyctosauridae [17]. The shaft gradually expands in diameter but steadily from the midpoint of the shaft, which is a feature of the Nyctosauridae [64]. However, since the femur was found in isolation, it cannot yet be known if it is also representative of *Epapatelo otyikokolo*, and therefore, the femur is more conservatively attributed here to the Pteranodontia.



**Figure 13.** Comparison of pteranodontian ulnae. (A,B) YPM 2499 and YPM 2497 *Pteranodon* sp. (adapted from Longrich et al. 2018 [17]), (C) NMP Ob 10-14 *Cretornis hlavaci* Frič 1881 (adapted from Averianov & Ekrt 2015 [21]), (D) MGUAN-PA650 *Epapatelo otyikokolo*, and (E) FSAC-OB 4 *Alcione elainus* (adapted from Longrich et al. 2018 [17]).

The MGUAN-PA660 metacarpal IV proximal end fragment appears to have had a subrectangular cross-section at the proximal end, a feature of the majority of the Pterodactyloidea. MGUAN-PA654, the distal shaft fragment of the metacarpal IV, appears to have a rounded-rectangular shape, which is a feature of the Pterodactyloidea, and also exhibits a surface between the distal condyles that lacks a median ridge. This material also shares traits with other pterodactyloids in that both metacarpals are elongated with no tapering on the distal shaft [18]. Furthermore, the wing digit IV first phalanx MGUAN-PA654, which was found in association with the metacarpal, has a pneumatic foramen on the ventral surface of the proximal end, a synapomorphy of ornithocheiroids [18]. Therefore, MGUAN-PA660 can be conservatively attributed to the Pterodactyloidea and MGUAN-PA654 to the Pteranodontia.

Beyond the shared morphological features with the Pteranodontia (including the Nyctosauridae), the Angolan assemblage is geochronologically congruent with the temporal range of the Nyctosauridae [17]. The relatively good three-dimensional preservation of the assemblage also indicates that their bones had not been transported harshly or far after death and thus remained taphonomically close to their habitats in life. Therefore, the presence of pterosaurs at Bentiaba indicates that they were preserved in their original marine environments, which is also in keeping with their piscivorous dietary preferences and in their being viewed behaviorally as analogs to large modern-day seabirds, as has been interpreted for *Pteranodon* and *Nyctosaurus* [58,65,66], spending time flying above open-water environments and diving to feed.

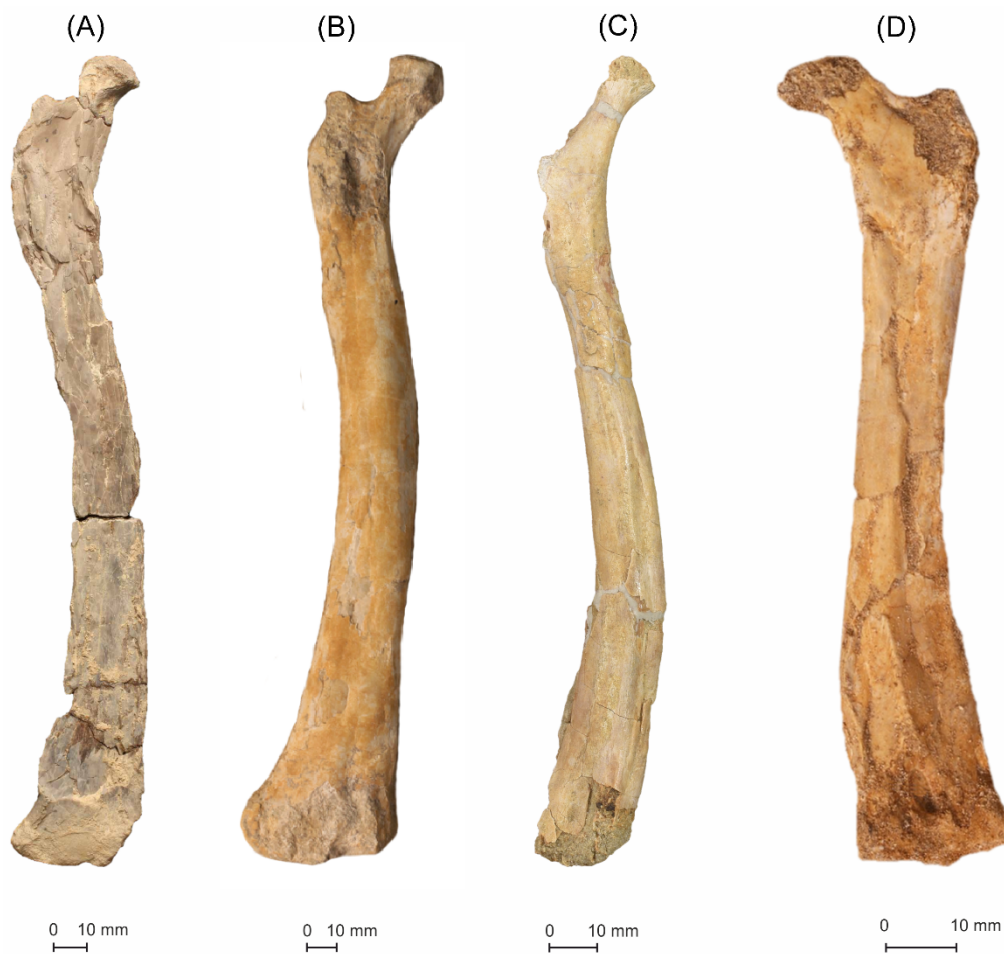


**Figure 14.** Comparison of pteranodontian femora. (A) YPM 2597 *Pteranodon* sp. (adapted from Longrich et al. 2018 [17]), (B) FSAC-OB 201 cf. *T. regalis* (adapted from Longrich et al. 2018 [17]), (C) MGUAN-PA163 Angola specimen, and (D) FSAC-OB 5 *Alcione elainus* (adapted from Longrich et al. 2018 [17]).

## 8. Conclusions

Pterosaur distribution reflects their volant lifestyle, and their rarity reflects the preservational fragility of their bones. Table S1 lists all known African pterosaur occurrences, with the closest Maastrichtian pterosaur-bearing locality to Bentiaba in Africa being in Senegal, roughly 4500 km to the northwest. The terrestrial fauna at Bentiaba, including its volant pterosaurs, was isolated from South America during the Late Cretaceous by a growing South Atlantic Ocean that was approximately 2700 km wide at the time, roughly half its current width [41].

The pterosaur sample from Bentiaba, integrated with previous interpretations of Bentiaba paleoecology, adds a significant dimension to the understanding of this marine site. At 71.64–71.40 Ma, Bentiaba is arguably the most precisely dated Late Cretaceous vertebrate fossil locality in Sub-Saharan Africa [41]. Taphonomic data presented by Strganac et al. 2015 [28], including nearest neighbor analysis, long axis orientation, completeness, and scavenge marks, indicate that the marine vertebrate carcasses at Bentiaba accumulated individually by attrition and were scavenged before burial. Reworking or concentration by currents are not significant factors at Bentiaba, except for occasional lag deposits concentrating small shark teeth and fish hash.

The distribution, occurrence, and completeness of the fourteen pterosaur bones (many individuals) at Bentiaba are consistent with this model. Table 1 shows that all specimens only comprise appendicular elements; no axial element is represented in any specimen.

Pterosaurs, as volant animals (and based on the scattered distribution and semi-articulated remains), almost certainly entered the sea as complete animals and were then predated and subsequently scavenged. All that remained to fossilize were the less palatable limb elements. We hypothesize that these pterosaurs entered the marine realm while feeding, much in the same way as modern seabirds such as gannets and brown pelicans (species that forage through plunge-diving [67–70]). In addition to taphonomic evidence and the abundance of top consumers, the distribution of pterosaurs remains is consistent with the interpretation of Bentiaba as representing a rich upwelling area that supported a diverse community along the Cretaceous African coast, including plunge-diving pterosaurs in their foraging areas.

The relative abundance of pterosaur material from the Mucuío Formation locality of Bentiaba is part of what makes this locality exceptional. The fourteen remarkably well-preserved pterosaur bones from this assemblage allow attributions to the Pterodactyloidea, the Pteranodontia, with one new genus and species, *Epapatelo otyikokolo*, and the recognition of a new apomorphy-based clade, the Aponyctosauria. Further fieldwork and sampling from this abundant locality would certainly yield much more insight into the paleobiodiversity of the Lower Maastrichtian, both globally and for Africa in particular.

**Supplementary Materials:** Supporting information can be downloaded at: <https://www.mdpi.com/article/10.3390/d14090741/s1>. [https://morphobank.org/index.php/MyProjects/List/select/project\\_id/3966](https://morphobank.org/index.php/MyProjects/List/select/project_id/3966). References [71–102] are cited in supplementary material.

**Author Contributions:** Conceptualization, A.E.F., L.L.J. and O.M.; methodology, A.E.F., B.A., L.L.J., M.J.P. and O.M.; software, A.E.F. and B.A.; validation, A.E.F., B.A., L.L.J., M.J.P., A.S.S., A.O.G. and O.M.; formal analysis, A.E.F. and B.A.; investigation, A.E.F., L.L.J., M.J.P., A.S.S. and O.M.; resources, L.L.J., M.J.P., A.S.S., A.O.G. and O.M.; data curation, A.E.F., M.J.P. and B.A.; writing—original draft preparation, A.E.F.; writing—review and editing, A.E.F., B.A., L.L.J., M.J.P., A.S.S. and O.M.; visualization, A.E.F., M.J.P. and A.S.S.; supervision, O.M., B.A. and L.L.J.; project administration, L.L.J.; funding acquisition, L.L.J., M.J.P., A.S.S. and O.M. All authors have read and agreed to the published version of the manuscript.

**Funding:** Projecto PaleoAngola has been supported by GeoBioTec-GeoBioSciences, GeoTechnologies and GeoEngineering NOVA [GeoBioCiências, GeoTecnologias e GeoEngenharias], grant UIDB/04035/2020, National Geographic Society (8039-06 and 8250-07), the Petroleum Research Fund of the American Chemical Society (45227-AC8), ISEM at SMU, The Royal Dutch Embassy in Luanda, TAP Airlines, KLM Royal Dutch Airlines, Sonangol EP, Esso Angola, the Perot Museum of Nature and Science, Naturalis Biodiversity Center, and The Saurus Institute.

**Acknowledgments:** Heartfelt thanks are extended to each member of Projecto PaleoAngola and to the “Dream Team” for their hard work and for their creative naming of the new species: Euridice Pacheco, Isabel Irene Dos Santos, Ana Soraya Marques, Celso Riquenga, Simão “Nimi” Diagrama, and Miguel Patrick Marx. Thank you to Jorge Arrimar, Maria Yoa, and Lueji Lara for the help with the relevant linguistics. Sincerest gratitude is extended to Carla Alexandra Tomás for her impeccable preparation and assistance; to Mike Eklund for his technical guidance; and to Miguel Moreno-Azanza, Eduardo Puertolas-Pascual, Chris Bennett, and Timothy Scott Myers for their thoughtful input on the manuscript. Thank you to Ana Fontoura and Jason Brizzolara for their paramount librarian services. Thank you to the ISEM at Southern Methodist University for providing scan funding and field support and to Calin Suteu for his expert digitization assistance. Thank you to Nick Longrich, Matyas Vremir, Olaf Dulfer and Pia Schucht, Carl Mehling, the staff of the Museu da Lourinhã, the Lourinhã PaleoTeam, and the Southern Methodist University and Universidade Nova de Lisboa staff.

**Conflicts of Interest:** The authors declare no conflict of interest.

## References

1. Barrett, P.M.; Butler, R.J.; Edwards, N.P.; Milner, A.R. Pterosaur distribution in time and space: An atlas. *Zitteliana* **2008**, *B28*, 61–107.
2. Kellner, A.W.A.; Mello, A.M.S.; Ford, T. A survey of pterosaurs from Africa with the description of a new specimen from Morocco. In *Paleontologia: Cenários da Vida*; Carvalho, I.S., Cassab, R.C.T., Schwanke, C., Carvalho, M.A., Fernandes, A.C.S., Eds.; Interciência: Rio de Janeiro, Brazil, 2007; pp. 257–267.

3. Mateus, O.; Callapez, P.M.; Polcyn, M.J.; Schulp, A.S.; Gonçalves, A.O.; Jacobs, L.L. The fossil record of biodiversity in Angola through time: A paleontological perspective. In *Biodiversity of Angola*; Huntley, B.J., Russo, V., Lages, F., Ferrand, N., Eds.; Springer International Publishing: Cham, Switzerland, 2019; pp. 53–76.
4. Araújo, R.; Polcyn, M.J.; Schulp, A.S.; Mateus, O.; Jacobs, L.L.; Gonçalves, A.O.; Morais, M.-L. A new elasmosaurid from the Early Maastrichtian of Angola and the implications of girdle morphology on swimming style in plesiosaurs. *Neth. J. Geosci.* **2015**, *94*, 109–120. [[CrossRef](#)]
5. Araújo, R.; Polcyn, M.J.; Lindgren, J.; Jacobs, L.L.; Schulp, A.S.; Mateus, O.; Gonçalves, A.O.; Morais, M.-L. New aristonectine elasmosaurid plesiosaur specimens from the Early Maastrichtian of Angola and comments on paedomorphism in plesiosaurs. *Neth. J. Geosci.* **2015**, *94*, 93–108. [[CrossRef](#)]
6. Jacobs, L.L.; Mateus, O.; Polcyn, M.J.; Schulp, A.S.; Antunes, M.T.; Morais, M.L.; Da Silva Tavares, T. The occurrence and geological setting of Cretaceous dinosaurs, mosasaurs, plesiosaurs, and turtles from Angola. *J. Paleontol. Soc. Korea* **2006**, *22*, 91–110.
7. Jacobs, L.L.; Mateus, O.; Polcyn, M.J.; Schulp, A.S.; Scotese, C.R.; Goswami, A.; Ferguson, K.M.; Robbins, J.; Vineyard, D.P.; Neto, A.B.; et al. Cretaceous paleogeography, paleoclimatology, and amniote biogeography of the low and mid-latitude South Atlantic Ocean. *Bull. Société Géologique Fr.* **2009**, *180*, 333–341. [[CrossRef](#)]
8. Marx, M.P.; Mateus, O.; Polcyn, M.J.; Schulp, A.S.; Gonçalves, A.O. The cranial anatomy and relationships of *Cardiocorax mukulu* (Plesiosauria: Elasmosauridae) from Bentiaba, Angola. *PLoS ONE* **2021**, *16*, 1–51.
9. Mateus, O.; Jacobs, L.; Polcyn, M.; Schulp, A.S.; Vineyard, D.; Buta Neto, A.; Antunes, M.T. The oldest African eucryptodiran turtle from the Cretaceous of Angola. *Acta Palaeontol. Pol.* **2009**, *54*, 581–588. [[CrossRef](#)]
10. Mateus, O.; Polcyn, M.J.; Jacobs, L.L.; Araújo, R.; Schulp, A.S.; Marinheiro, J.; Pereira, B.; Vineyard, D. Cretaceous amniotes from Angola: Dinosaurs, pterosaurs, mosasaurs, plesiosaurs, and turtles. In *Actas de V Jornadas Internacionales sobre Paleontología de Dinosaurios y su Entorno*; Hurtado, P.H., Fernández-Baldor, F.T., Canudo Sanagustín, J.I., Eds.; Colectivo Arqueológico y Paleontológico de Salas, C.A.S.: Burgos, Spain, 2012; pp. 71–105.
11. Polcyn, M.J.; Jacobs, L.L.; Schulp, A.S.; Mateus, O. The North African mosasaur *Globidens phosphaticus* from the Maastrichtian of Angola. *Hist. Biol.* **2010**, *22*, 175–185. [[CrossRef](#)]
12. Schulp, A.S.; Polcyn, M.J.; Mateus, O.; Jacobs, L.L.; Morais, M.L.; da Silva Tavares, T. New mosasaur material from the Maastrichtian of Angola, with notes on the phylogeny, distribution and palaeoecology of the genus *Prognathodon*. *Publ. Van Het Nat. Genoot. Limbg. Reeks XLV Aflevering* **2006**, *1*, 57–67.
13. Schulp, A.S.; Polcyn, M.J.; Mateus, O.; Jacobs, L.L.; Morais, M.L. A new species of *Prognathodon* (Squamata, Mosasauridae) from the Maastrichtian of Angola, and the affinities of the mosasaur genus *Liodon*. In Proceedings of the Second Mosasaur Meeting, Fort Hays Studies Special Issue, Hays, KS, USA, 3–6 May 2007; pp. 1–12.
14. O’Leary, M.A.; Kaufman, S.G. MorphoBank 3.0: Web Application for Morphological Phylogenetics and Taxonomy. 2012. Available online: <http://morphobank.org/permalink/?3966> (accessed on 24 July 2022).
15. Goloboff, P.; Catalano, S. T.N.T., version 1.5, with a full implementation of phylogenetic morphometrics [computer software]. *Cladistics* **2016**, *32*, 221–238. [[CrossRef](#)]
16. Goloboff, P.A.; Farris, J.S.; Nixon, K.C. T.N.T., a free program for phylogenetic analysis. *Cladistics* **2008**, *24*, 774–786. [[CrossRef](#)]
17. Longrich, N.R.; Martill, D.M.; Andres, B. Late Maastrichtian pterosaurs from North Africa and mass extinction of Pterosauria at the Cretaceous–Paleogene boundary. *PLoS Biol.* **2018**, *16*, e2001663.
18. Andres, B.; Clark, J.; Xu, X. The earliest pterodactyloid and the origin of the group. *Curr. Biol.* **2014**, *24*, 1011–1016. [[CrossRef](#)] [[PubMed](#)]
19. Broom, R. Note on *Mesosuchus browni*, Watson and on a new South African Triassic pseudosuchian (*Euparkeria capensis*). *Rec. Albany Mus* **1913**, *2*, 394–396.
20. Frič, A. O zkamenělem pt aku Chocěnském. *Vesmír* **1881**, *10*, 232–233.
21. Averianov, A.; Ekrt, B. *Cretornis hlavaci* Frič, 1881 from the Upper Cretaceous of Czech Republic (Pterosauria, Azhdarchoidea). *Cretac. Res.* **2015**, *55*, 164–175. [[CrossRef](#)]
22. Varricchio, D.J. A new bird from the Upper Cretaceous Two Medicine Formation of Montana. *Can. J. Earth Sci.* **2002**, *39*, 19–26. [[CrossRef](#)]
23. Lamm, E. Preparation and sectioning of specimens. In *Bone Histology of Fossil Tetrapods*; Padian, K., Lamm, E., Eds.; University of California Press: Berkeley, CA, USA, 2013; pp. 55–160.
24. Sampson, S.D. Predatory Dinosaur Remains from Madagascar: Implications for the Cretaceous biogeography of Gondwana. *Science* **1998**, *280*, 1048–1051. [[CrossRef](#)]
25. Benton, M.J.; Bouaziz, S.; Buffetaut, E.; Martill, D.; Ouaja, M.; Soussi, M.; Truema, C. Dinosaurs and other fossil vertebrates from fluvial deposits in the lower Cretaceous of southern Tunisia. *Palaeogeogr. Palaeoclimatol. Palaeoecol.* **2000**, *157*, 227–246. [[CrossRef](#)]
26. Strganac, C.; Salminen, J.; Jacobs, L.L.; Polcyn, M.J.; Ferguson, K.M.; Mateus, O.; Schulp, A.S.; Morais, M.L.; Tavares, T.S.; Gonçalves, A.O. Carbon isotope stratigraphy, magnetostratigraphy, and <sup>40</sup>Ar/<sup>39</sup>Ar age of the Cretaceous South Atlantic coast, Namibe Basin, Angola. *J. Afr. Earth Sci.* **2014**, *99*, 452–462. [[CrossRef](#)]
27. U.S. Geological Survey. Geological Map of Africa [Map on the Internet]. 2002. Available online: <http://www.uni-koeln.de/sfb389/e/e1/> (accessed on 24 July 2022).

28. Strganac, C.; Jacobs, L.L.; Polcyn, M.J.; Mateus, O.; Myers, T.S.; Salminen, J.; May, S.R.; Araújo, R.; Ferguson, K.M.; Gonçalves, A.O.; et al. Geological setting and paleoecology of the Upper Cretaceous Bench 19 marine vertebrate bonebed at Bentiaba, Angola. *Neth. J. Geosci.—Geol. En Mijnb.* **2015**, *94*, 121–136. [[CrossRef](#)]
29. Strganac, C.; Jacobs, L.L.; Polcyn, M.J.; Ferguson, K.M.; Mateus, O.; Gonçalves, A.O.; Morais, M.-L.; da Silva Tavares, T. Stable oxygen isotope chemostratigraphy and paleotemperature regime of mosasaurs at Bentiaba, Angola. *Neth. J. Geosci.—Geol. En Mijnb.* **2015**, *94*, 137–143. [[CrossRef](#)]
30. Marsh, O.C. Principal characters of American pterodactyls. *Am. J. Sci.* **1876**, *3*, 479–480. [[CrossRef](#)]
31. Currey, J.D.; Alexander, R.M. The thickness of the walls of tubular bones. *J. Zool.* **2009**, *206*, 453–468. [[CrossRef](#)]
32. Bennett, S.C. Morphological evolution of the pectoral girdle of pterosaurs: Myology and function. *Geol. Soc. Lond. Spec. Publ.* **2003**, *217*, 191–215. [[CrossRef](#)]
33. Bennett, S.C. The osteology and functional morphology of the Late Cretaceous pterosaur *Pteranodon*. Part I. General description and osteology. *Paleontographica A* **2001**, *260*, 1–112. [[CrossRef](#)]
34. Bennett, S.C. The ontogeny of *Pteranodon* and other pterosaurs. *Paleobiol. Winter* **1993**, *19*, 92–106. [[CrossRef](#)]
35. Owen, R. Report on British Fossil Reptiles, Part II. In Proceedings of the 11th Meeting of the British Association for the Advancement of Science, Plymouth, UK, 24 July 1841; pp. 60–204.
36. Andres, B.; Padian, K.; Pterosauria, R. Owen 1842. In *Phylonyms*; de Queiroz, K., Cantino, P.D., Gauthier, J.A., Eds.; CRC Press: Boca Raton, FL, USA, 2020; pp. 1201–1204.
37. Plieninger, F. Beiträge Zur Kenntnis der Flugsaurier. *Paläontographica* **1901**, *48*, 65–90.
38. Andres, B.; Padian, K.; Pterodactyloidea, F. Plieninger 1901. E. In *Phylonyms*; de Queiroz, K., Cantino, P.D., Gauthier, J.A., Eds.; CRC Press: Boca Raton, FL, USA, 2020; pp. 1205–1207.
39. Unwin, D.M. On the Phylogeny and Evolutionary History of Pterosaurs. In *Geological Society*; Special Publications: London, UK, 2003; Volume 217, pp. 139–190.
40. Padres missionarios da Congregação do Espírito Santo e do Sagrado Coração de Maria. In *Diccionario Portuguez-Olunyaneka*; Typographia da Missão: Huilla, Colombia, 1896.
41. Jacobs, L.L.; Polcyn, M.J.; Mateus, O.; Schulp, A.S.; Gonçalves, A.O.; Morais, M.L. Post-Gondwana Africa and the vertebrate history of the Angolan Atlantic coast. *Mem. Mus. Vic.* **2016**, *74*, 343–362. [[CrossRef](#)]
42. Averianov, A.O.; Arkhangelsky, M.S.; Pervushov, E.M. A new Late Cretaceous azhdarchid (Pterosauria, Azhdarchidae) from the Volga Region. *Paleontol. J.* **2008**, *42*, 634–642. [[CrossRef](#)]
43. Andres, B.; Myers, T.S. Lone Star pterosaurs. *Earth Environ. Sci. Trans. R. Soc. Edinb.* **2013**, *103*, 383–398. [[CrossRef](#)]
44. Frey, E.; Buchy, M.C.; Stinnesbeck, W.; González, A.G.; Stefano, A. *Muzquizopteryx coahuilensis* n.g., sp. nov., a nyctosaurid pterosaur with soft tissue preservation from the Coniacian (Late Cretaceous) of northeast Mexico (Coahuila). *Oryctos* **2006**, *6*, 19–39.
45. Bennett, S.C. The osteology and functional morphology of the Late Cretaceous pterosaur *Pteranodon*. Part II. Size and functional morphology. *Paleontographica A* **2001**, *260*, 115–153. [[CrossRef](#)]
46. Cox, R.M.; Butler, M.A.; John-Alder, H.B. The evolution of sexual size dimorphism in reptiles. In *Sex, Size and Gender Roles: Evolutionary Studies of Sexual Size Dimorphism*; Fairbairn, D.J., Blanckenhorn, W.U., Székely, T., Eds.; Oxford University Press: Oxford, UK, 2007; pp. 38–49.
47. Padian, K. Bone histology determines identification of a new fossil taxon of pterosaur (Reptilia: Archosauria). *Comptes Rendus L'académie Des Sci. Vie Des Sci.* **1995**, *320*, 77–84.
48. de Ricqlès, A.J.; Padian, K.; Horner, J.R.; Francillon-Vieillot, H. Palaeohistology of the bones of pterosaurs (Reptilia: Archosauria): Anatomy, ontogeny, and biomechanical implications. *Zool. J. Linn. Soc.* **2000**, *129*, 349–385. [[CrossRef](#)]
49. Steel, L. The palaeohistology of pterosaur bone: An overview. *Zitteliana: Int. J. Paleontol. Geobiol.* **2008**, *B28*, 109–125.
50. Prondvai, E.; Stein, K.; Ósi, A.; Sander, M.P. Life history of *Rhamphorhynchus* inferred from bone histology and the diversity of pterosaurian growth strategies. Soares D, editor. *PLoS ONE* **2012**, *7*, e31392. [[CrossRef](#)]
51. Padian, K.; Lamm, E.T.; Werning, S. Selection of specimens. In *Bone Histology of Fossil Tetrapods*; Padian, K., Lamm, E., Eds.; University of California Press: Berkeley, CA, USA, 2013; pp. 54–76.
52. de Margerie, E. Laminar bone as an adaptation to torsional loads in flapping flight. *J. Anat.* **2002**, *201*, 521–526. [[CrossRef](#)]
53. Chinsamy-Turan, A.; Codorniu, L.; Chiappe, L. Paleobiological implications of the bone histology of *Pterodaustro guinazui*. *Anat. Rec.* **2009**, *292*, 1462–1477. [[CrossRef](#)]
54. Cullinane, D.M. The role of osteocytes in bone regulation: Mineral homeostasis versus mechanoreception. *J. Musculoskelet. Neuronal Interact.* **2002**, *2*, 242–244.
55. Chinsamy-Turan, A.; Codorniu, L.; Chiappe, L. Developmental growth patterns of the filter-feeder pterosaur, *Pterodaustro guinazui*. *Biol. Lett.* **2008**, *4*, 282–285. [[CrossRef](#)] [[PubMed](#)]
56. Woodward, H.N.; Padian, K.; Lee, A.H. Skeletochronology. In *Bone Histology of Fossil Tetrapods*; Padian, K., Lamm, E., Eds.; University of California Press: Berkeley, CA, USA, 2013; pp. 195–216.
57. Sayão, J.M. Histovariability in bones of two pterodactyloid pterosaurs from the Santana Formation, Araripe Basin, Brazil: Preliminary results. *Geol. Soc. Lond. Spec. Publ.* **2003**, *217*, 335–342. [[CrossRef](#)]
58. Bennett, S.C. New smallest specimen of the pterosaur *Pteranodon* and ontogenetic niches in pterosaurs. *J. Paleontol.* **2018**, *92*, 254–271. [[CrossRef](#)]

59. Lee, A.H.; Huttenlocker, A.K.; Padian, K.; Woodward, H.N. Analysis of growth rates. In *Bone Histology of Fossil Tetrapods*; Padian, K., Lamm, E., Eds.; University of California Press: Berkeley, CA, USA, 2013; pp. 217–251.
60. Rodrigues, T.W.A.; Kellner, A.W.A.; Mader, B.A.; Russell, D. New pterosaur specimens from the Kem Madder beds (Upper Cretaceous, Cenomanian) of Morocco. *Riv. Ital. Paleontol. E Stratigr.* **2011**, *117*, 149–160.
61. Andres, B.; Ji, Q. A new pterosaur from the Liaoning province of China, the phylogeny of the Pterodactyloidea, and convergence in their cervical vertebrae. *Palaeontology* **2008**, *51*, 453–469. [[CrossRef](#)]
62. Bennett, S.C. Taxonomy and systematics of the Late Cretaceous pterosaur *Pteranodon* (Pterosauria, Pterodactyloidea). *Occas. Pap. Mus. Nat. Hist. Univ. Kans. Lawrence* **1994**, *169*, 1–70.
63. Claessens, L.P.A.M.; O'Connor, P.M.; Unwin, D.M. Respiratory evolution facilitated the origin of pterosaur flight and aerial gigantism. Sereno P, editor. *PLoS ONE* **2009**, *4*, e4497. [[CrossRef](#)]
64. Williston, S.W.; Museum, F.C. *On the Osteology of Nyctosaurus (Nyctodactylus), with Notes on American Pterosaurs*; Field Columbian Museum Geological Series; Field Columbian Museum: Chicago, IL, USA, 1903.
65. Brower, J.C. The aerodynamics of *Pteranodon* and *Nyctosaurus*, two large pterosaurs from the Upper Cretaceous of Kansas. *J. Vertebr. Paleontol.* **1983**, *3*, 84–124. [[CrossRef](#)]
66. Witton, M.P.; Habib, M.B. On the size and flight diversity of giant pterosaurs, the use of birds as pterosaur analogues and comments on pterosaur flightlessness. *PLoS ONE* **2010**, *5*, e13982. [[CrossRef](#)] [[PubMed](#)]
67. Brumm, H.; Teschke, I. Juvenile Galápagos Pelicans increase their foraging success by copying adult behaviour. *PLoS ONE* **2012**, *7*, e51881. [[CrossRef](#)]
68. Garthe, S.; Guse, N.; Montevicchi, W.A.; Rail, J.F.; Grégoire, F. The daily catch: Flight altitude and diving behavior of northern gannets feeding on Atlantic mackerel. *J. Sea Res.* **2014**, *85*, 456–462. [[CrossRef](#)]
69. Geary, B.; Leberg, P.L.; Purcell, K.M.; Walter, S.T.; Karubian, J. Breeding brown pelicans improve foraging performance as energetic needs rise. *Sci. Rep.* **2020**, *10*, 1–9.
70. Schreiber, R.W.; Woolfenden, G.E.; Curtsinger, W.E. Prey capture by the brown pelican. *Auk* **1975**, *92*, 649–654. [[CrossRef](#)]
71. Ntamak-Nida, M.J.; Ketchemen-Tandia, B.; Ewane, R.V.; Lissok, J.P.; Courville, P. Nouvelles données sur les mollusques et autres macro-organismes campaniens de Sikoum (centre-est du sous bassin de Douala-Cameroun): Intérêts bio-chronologiques et paléo-écologiques. *Afr. Geosci. Rev.* **2006**, *13*, 385–394.
72. Swinton, W.E. A Cretaceous pterosaur from the Belgian Congo. *Bull. Soc. Belge Geol. Paléont. Hydr. Liège* **1948**, *77*, 234–238.
73. Wellnhofer, P.; Buffetaut, E. Pterosaur remains from the Cretaceous of Morocco. *Paläontologische Z.* **1999**, *73*, 133–142. [[CrossRef](#)]
74. O'Connor, P.M.; Sertich, J.J.W.; Manthi, F.K. A pterodactyloid pterosaur from the Upper Cretaceous Lapurr sandstone, West Turkana, Kenya. *An. Acad. Bras. Ciências* **2011**, *83*, 309–315. [[CrossRef](#)]
75. Dal Sasso, C.; Pasini, G. First record of pterosaurs (Diapsida, Archosauromorpha, Pterosauria) in the Middle Jurassic of Madagascar. *Atti Della Soc. Ital. Sci. Nat. E Del Mus. Civ. Stor. Nat. Milano* **2003**, *144*, 281–296.
76. Flynn, J.J.; Fox, S.R.; Parrish, J.; Ranivoharimanana, L.; Wyss, A.R. Assessing diversity and paleoecology of a Middle Jurassic microvertebrate assemblage from Madagascar. *New Mex. Mus. Nat. Hist. Sci. Bull.* **2006**, *37*, 476–489.
77. Kellner, A.W.A.; Mader, B.J. Archosaur teeth from the Cretaceous of Morocco. *J. Paleontol.* **1997**, *71*, 525–527. [[CrossRef](#)]
78. Mader, B.; Kellner, A.W.A. A new anhanguerid pterosaur from the Cretaceous of Morocco. *Bol. Do Mus. Nac.* **1999**, *45*, 1–11.
79. Kellner, A.W.A.; Mader, B.J. First report of Pterosauria (Pterodactyloidea, Azhdarchidae) from Cretaceous rocks of Morocco (Abstract). *J. Vertebr. Paleontol.* **1996**, *16*, 45A.
80. Martill, D.M.; Smith, R.; Unwin, D.M.; Kao, A.; McPhee, J.; Ibrahim, N. A new tapejarid (Pterosauria, Azhdarchoidea) from the mid-Cretaceous Kem Boleti beds of Takmout, southern Morocco. *Cretac. Res.* **2020**, *112*, 104424. [[CrossRef](#)]
81. Ibrahim, N.; Unwin, D.M.; Martill, D.M.; Baidder, L.; Zouhri, S. A new pterosaur (Pterodactyloidea: Azhdarchidae) from the Upper Cretaceous of Morocco. Farke AA, editor. *PLoS ONE* **2010**, *5*, e10875. [[CrossRef](#)] [[PubMed](#)]
82. Martill, D.M.; Ibrahim, N. An unusual modification of the jaws in cf. *Alanqa*, a mid-Cretaceous azhdarchid pterosaur from the Kem Alana beds of Morocco. *Cretac. Res.* **2015**, *53*, 59–67.
83. Martill, D.M.; Unwin, D.M.; Ibrahim, N.; Longrich, N. A new edentulous pterosaur from the Cretaceous Kem Alana beds of south eastern Morocco. *Cretac. Res.* **2018**, *84*, 1–12. [[CrossRef](#)]
84. Jacobs, M.L.; Martill, D.M.; Ibrahim, N.; Longrich, N. A new species of *Coloborhynchus* (Pterosauria, Ornithocheiridae) from the mid-Cretaceous of North Africa. *Cretac. Res.* **2019**, *95*, 77–88. [[CrossRef](#)]
85. Jacobs, M.L.; Martill, D.M.; Unwin, D.M.; Ibrahim, N.; Zouhri, S.; Longrich, N. New toothed pterosaurs (Pterosauria: Ornithocheiridae) from the middle Cretaceous Kem Alana beds of Morocco and implications for pterosaur palaeobiogeography and diversity. *Cretac. Res.* **2020**, *110*, 1–16. [[CrossRef](#)]
86. McPhee, J.; Ibrahim, N.; Kao, A.; Unwin, D.M.; Smith, R.; Martill, D.M. A new ?chaoyangopterid (Pterosauria: Pterodactyloidea) from the Cretaceous Kem paleobiogeography beds of southern Morocco. *Cretac. Res.* **2020**, *110*, 104410. [[CrossRef](#)]
87. Knoll, F. Pterosaurs from the lower Cretaceous (?Berriasian) of Anoual, Morocco. *Ann. De Paléontologie* **2000**, *86*, 157–164. [[CrossRef](#)]
88. Suberbiola, X.P.; Bardet, N.; Jouve, S.; Iarochène, M.; Bouya, B.; Amaghazaz, M. A new azhdarchid pterosaur from the Late Cretaceous phosphates of Morocco. *Geol. Soc. Lond. Spec. Publ.* **2003**, *217*, 79–90. [[CrossRef](#)]
89. Smith, R.E.; Martill, D.M.; Kao, A.; Zouhri, S.; Longrich, N. A long-billed, possible probe-feeding pterosaur (Pterodactyloidea: ?Azhdarchoidea) from the mid-Cretaceous of Morocco, North Africa. *Cretac. Res.* **2020**, 104643. [[CrossRef](#)]

90. Labita, C.; Martill, D.M.M. An articulated pterosaur wing from the Upper Cretaceous (Maastrichtian) phosphates of Morocco. *Cretac. Res.* **2021**, *119*, 1–15. [[CrossRef](#)]
91. Sereno, P.C.; Brusatte, S.L. Basal abelisaurid and carcharodontosaurid theropods from the lower Cretaceous Elrhaz Formation of Niger. *Acta Palaeontol. Pol.* **2008**, *53*, 15–46. [[CrossRef](#)]
92. Blackburn, D.C. Two Early Cretaceous pterosaurs from Africa (Abstract). *J. Vertebr. Paleontol.* **2002**, *22* (Suppl. S3), 37A.
93. Montillet, J.; Lappartient, J.R.; Taquet, P. Un ptérosaure géant dans le Crétacé supérieur de Paki (Sénégal). *C. R. Acad. Sic. Paris* **1982**, *295*, 167–172.
94. Blackbeard, M.; Yates, A. The taphonomy of an Early Jurassic dinosaur bonebed in the Northern Free State (South Africa). *J. Vertebr. Paleontol.* **2007**, *27* (Suppl. S3), 49A.
95. Reck, H. Die deutschostafrikanischen flugsaurier. *Cent. Für Mineral. Geol. Und Paläontologie* **1931**, *7*, 321–336.
96. Unwin, D.M.; Heinrich, W.-D. On a pterosaur jaw from the upper Jurassic of Tendaguru (Tanzania). *Foss. Rec.* **1999**, *2*, 121–134. [[CrossRef](#)]
97. Galton, P.M. Avian-like tibiotarsi of pterodactyls (Reptilia: Pterosauria) from the upper Jurassic of East Africa. *Paläontologische Z.* **1980**, *54*, 331–342. [[CrossRef](#)]
98. Sayão, J.M.; Kellner, A.W.A. New data on the pterosaur fauna from Tendaguru (Tanzania), Upper Jurassic, Africa. *J. Vertebr. Paleontol.* **2001**, *21* (Suppl. S3), 97A.
99. Costa, F.R.; Kellner, A.W.A. On two pterosaur humeri from the Tendaguru beds (upper Jurassic, Tanzania). *An. Acad. Bras. Ciências* **2009**, *81*, 813–818. [[CrossRef](#)] [[PubMed](#)]
100. Costa, F.R.; Sayão, J.M.; Kellner, A.W.A. New pterosaur material from the upper Jurassic of Tendaguru (Tanzania), Africa. *Hist. Biol.* **2015**, *27*, 646–655. [[CrossRef](#)]
101. Fanti, F.; Contessi, M.; Franchi, F. The “Continental Intercalaire” of southern Tunisia: Stratigraphy, paleontology, and paleoecology. *J. Afr. Earth Sci.* **2012**, *73–74*, 1–23. [[CrossRef](#)]
102. Martill, D.M.; Ibrahim, N.; Bouaziz, S. A giant pterosaur in the Early Cretaceous (Albian) of Tunisia. *J. Afr. Earth Sci.* **2018**, *147*, 331–337. [[CrossRef](#)]